Buoyant Flows in Vertical Channels Relating to Smoke Movement in High-Rise Building Fires

Thesis by

Noel Lakshman Benedict

In Partial Fulfillment of the Requirements

for the Degree of

Doctor of Philosophy

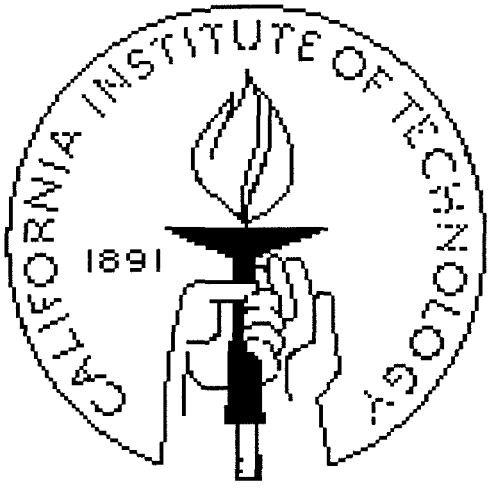

California Institute of Technology

Pasadena, California

1999

(Submitted September 10, 1998)

Acknowledgements

I am much indebted to my advisor Professor Melany Hunt for her guidance and support throughout my stay at Caltech. She was my academic advisor during my first year here and later "adopted" me as one of her advisees during my fourth year. She patiently read the several revisions of my thesis. I gratefully acknowledge her counsel and encouragement.

I also owe a debt of gratitude to Professor Ed Zukoski who was my thesis advisor for three years until he passed away in May 1997. He introduced me to the subject of fire science and was a wonderful mentor and a great inspiration to me. His cheerful and uplifting personality will be missed very much.

My sincere thanks to the late Professor Toshi Kubota for his help, particularly with the analytical part of my study. I also thank Professor Frank Marble for all the informative discussions that we had. The assistance of Professors Fred Culick and Dave Goodwin who were on my thesis committee and provided several useful suggestions is appreciated.

Several people made my stay at Caltech an enjoyable one; Rajesh Kedia, Joe Sivo, Sayuri Desai, Aseem Mehta, Kanchana Nanayakkara, Ramya Dissanayake, Ashok Tripathi, Venkata Natarajan, Joe Christopherson, Ryan Mackey, Pradeep Guduru, Muruhan Rathinam, Ayhan Irfonoglu and Yen Phan to name a few. Bob Uy, Anna Karion, Simon Yeung, Roberto Zenit, Qiao Lin, provided technical support with the writing of this thesis. My thanks also to Sudipto Sur, Tricia Waniewski, Clancey Rowley, Martha Gallivan and Jeff Eldredge

I also appreciate the help of Steve Palm and Vahe Mammakunian with the design of my experiment. My other colleagues at the Jet Propulsion Center; Patrick Lemieux, Chris Cadou, Victor Burnley, Windsor Lin, Tom Zsak, Winston Pun, Grant Swenson, Donald Kendrick, and Kevin Moore provided advice and support in various ways. My thanks also to Dorothy Eckerman, Marionne Kirk, Dana Young, Jackie Beard, Connie

Yehle and Lynn Burgess for their help.

I am also grateful to Tamara Withana, Surinder Jhaj and all our other friends whose support and encouragement were invaluable.

Finally my grateful thanks to my parents, my parents-in-law and my extended family. My wife Lasanthi has been by my constant inspiration and I thank her for her love and support. We have been through a lot together and the most difficult times have been the the three miscarriages that we went through. This thesis is dedicated to Lasanthi and our three babies who were never born.

This study was made possible by a grant from the National Institute of Science and Technology.

Abstract

This experimental study is motivated by the widespread loss of life and property due to accidental fires in high rise buildings, and investigates the progress of hot, toxic, products during such fires. The *Stack Effect* and *Turbulent Mixing*, two of the primary factors responsible for smoke movement within tall buildings are the focus of this study. The results of this investigation could be used for the development of fire modeling codes that simulate high-rise building fires.

The experiments involve a 2.6 m tall square shaft with various cross sections and openings. The shaft was situated above a large temperature controlled hot air reservoir, and the two chambers were initially separated by a partition. At the start of the experiment the partition was removed in a rapid horizontal motion and the hot and cold gases were allowed to mix. For the shafts with openings, the gases were withdrawn from the apertures at different rates with the Reynolds number varying between 600 and 7200. The temperature of the gas and wall, and the heat transfer to the wall were measured as functions of time at various locations in the shaft. Additionally, hot wire anemometry techniques were used to obtain velocity data in the channel. Some experiments involved monitoring a tracer gas in the vertical channel. Simple one-dimensional analytical modeling was performed to validate the experimental results.

The experiments indicated an initial transient period followed by a "pseudo steady state." At each elevation measured the cross-section averaged gas temperature, reached and fluctuated about a steady state value soon after the initial front of hot gas arrived at that location. For the closed channel experiments, the front arrival time was a function of the initial density ratio, the shaft width, and the gravitational constant.

The tracer gas trials suggested that the molecular diffusion was insignificant in comparison to the turbulent mixing. For the closed channels the observed velocity

fluctuations were the same order of magnitude as the mean velocities. The time averaged heat transfer coefficient was weakly dependent on the initial reservoir temperature.

The vented shaft experiments indicated that the front propagation times are significantly affected by openings in the shaft and that the effect is more pronounced the higher the vents are located. The venting caused a significant rise in the steady state temperatures, and a reduction in both the temperature and velocity fluctuations. The local Nusselt number was independent of the Reynolds number and a function only of the Rayleigh number, indicating that the heat transfer was dominated by free convection effects.

The predictions made by the one dimensional analytical model agreed reasonably well with the experiments, particularly in the case of the closed channel.

Contents

List of Figures

Nomenclature

Roman symbols

C = concentration

C^* = normalized concentration

c_p = specific heat at constant pressure

CTA = constant temperature anemometer

g = gravitational constant, 9.81 m/s^2

Gr = Grashof number

H = channel height

h = heat transfer coefficient

H/w = aspect ratio

k = thermal conductivity

k_H = eddy conductivity

l = vertical scale of mixing

LFE = laminar flow element

$\dot{m}$= mass flow withdrawal rate

Nu = Nusselt number

P = pressure

Pr = Prandtl number

q_w = heat flux to the wall

Q = volumetric flow rate

r = distance from wall

R_s = sensor resistance

Ra = Rayleigh number

Re_w = Reynolds number

t = time

T = instantaneous gas temperature

T_{ss} = steady state time-averaged temperature

T_w = wall temperature

$\overline{T}$ = mean component of temperature

T' = fluctuating component of temperature

T^* = normalized temperature

u = velocity

u_{ave}= cross-section averaged velocity

$\overline{u}$ = mean velocity

u' = velocity fluctuation

u_1 = characteristic velocity

V_{obs}= observed voltage

V = corrected voltage

w = channel width

x = horizontal coordinate

y = horizontal coordinate

z_1 = height above neutral plane

z = elevation from bottom of shaft

Greek symbols

α = molecular thermal diffusivity

β = volumetric thermal expansion coefficient

ϵ_H = eddy thermal diffusivity

λ = mixing length

μ = dynamic viscosity ν = kinematic viscosity

ρ = density

ΔP = pressure difference

$\Delta\rho$ = density difference

τ = normalized temperature

ζ = normalized elevation

constants: $a, a_1, a_2, b_1, b_2, c, c_1, c_2, c_{bg}, c_v, c_q, \gamma$

subscripts

avg = average

f = final

h = reservoir (hot)

i = initial or internal

lfe = measured at laminar flow element

np = neutral plane

o = external

w = based on width

z = based on length

Chapter 1 Introduction

1.1 Motivation

Fires, through the combustion of fuels, provide a substantial part of the industrial world's energy requirements. However, accidental fires kill thousands of people and cause widespread destruction to property. In 1996, US fire departments responded to 1.975 billion fires (Karter, 1997). About 30% of these occurred in structures. Structure fires caused about 4,000 deaths, over 20,000 injuries and $7.9 billion in property damage.

High-rise buildings are found in most parts of the world and are often constructed to meet the needs of a growing urban population. Fires in these tall buildings often have consequences different from those in smaller structures. When a fire starts in a high-rise building, resulting smoke and fumes can proceed through stairwells, elevator shafts, and heating ducts to parts of the building remote from the fire in a short time.

The National Fire Protection Association (NFPA) maintains a list of fires from around the world, and publishes various statistical information regarding losses resulting from those fires in the NFPA Journal. Some of the more disastrous fires that have resulted in large losses in terms of life and property are catalogued in Lyons (1985). Zicherman et al. (1992) lists case studies of several high-rise fires that transpired between 1967 and 1989. The November 1980 conflagration, in the MGM Grand hotel in Las Vegas, Nevada, is an example of the potential damage in a high-rise. The fire started in a deli on the first floor due to an electrical short circuit, and in less than a few minutes the entire first floor was engulfed in flames (Emmons, 1988). Toxic fumes then moved up to the other floors of the 23 story building through expansion joints in the buildings, the elevator shafts and air supply ducts. Although the fire department crews arrived within minutes of the fire being detected, 85 people lost their lives. The majority of these deaths were due to smoke inhalation.

The fire protection engineer must be concerned with controlling the movement of smoke in the event of a fire. Since fire escape routes in a tall building may be longer than usual, and due to the possibility of excessive smoke build-up on some floors, high-rise buildings usually have to conform to special codes and standards for fire safety (Hall, 1997). The installation of automatic sprinkler systems, the pressurization of stairwells and the use of fire resistive building materials are possible examples. These safety features include provisions for protecting occupants of buildings from smoke. This study attempts to enhance the understanding of how smoke propagates within a tall building and thereby provide insight into the design of building fire codes.

1.2 Characteristics of a High-Rise Fire

The high-rise fire in its early stages is often similar to any other building fire, in the sense that it is confined to a small area where it started. If a continuous supply of fuel and air exists, heat from the flames is transferred, primarily by convection and radiation, to other objects in the room of origin. If the fire continues to grow unchecked, a condition known as flashover may occur. This is usually indicated by a sudden rise in the room temperature and entire compartment being involved in the fire (Zicherman et al., 1992). Though pre-flashover fires can be harmful, post-flashover fires are extremely dangerous and are more likely to spread to other compartments.

The fire gases often contain large amounts of carbon monoxide (CO), which is a product of incomplete combustion that occurs when a fire is deprived of oxygen. CO is the most lethal of the toxic gases produced in a fire since it enters the bloodstream and replaces oxygen in the blood cells causing death by suffocation. Hydrogen chloride, hydrogen cyanide, formaldehyde, acetaldehyde and acrolein are a few of the other noxious gases produced by either incomplete combustion or chemical decomposition (pyrolysis) of the burning material. The inhalation of toxic fire products is the primary cause of fire related deaths.

Smoke and toxic fumes produced by the fire propagate from the fire compartment to other parts of the building. The factors responsible for the movement of smoke

during a fire in a tall building are: the stack effect, turbulent mixing, the air handling system and external wind (Drysdale, 1985). Each of these factors is briefly described below.

Stack Effect: A difference in temperature between the interior and exterior of a building that contains tall vertical shafts generates the stack effect (also called the chimney effect). An air flow path between the shaft and the exterior is also required and is almost always present due to small leaks near the windows and doors of buildings. These temperature differences give rise to buoyancy induced pressure differences.

Consider, for example, a building heated during winter; the neutral pressure plane is the vertical location where the pressure inside and outside the building is the same, and is usually near the mid-height for a building with evenly distributed leaks. If the pressure at the neutral plane is P_{np}, the internal pressure at a height z_1 above it is

$$P_i(y) = P_{np} - \rho_i g z_1 \tag{1.1}$$

And the external pressure at the same height is

$$P_o(y) = P_{np} - \rho_o g z_1 \tag{1.2}$$

where ρ_i and ρ_o are the densities inside and outside the shaft. Hence the pressure difference is,

$$\Delta P(y) = P_i - P_o = (\rho_o - \rho_i) g z_1 \tag{1.3}$$

Therefore, during a fire, toxic gases above the neutral plane can flow out of the vertical shaft, while gases below the neutral plane can flow into the shaft as shown in fig. 1.1. Thus, fire products can be transported extremely rapidly within a building. In fact, smoke movement from a building fire can be dominated by the stack effect (Zicherman et al., 1992).

The situation illustrated in fig. 1.1 is called the normal stack effect. However,

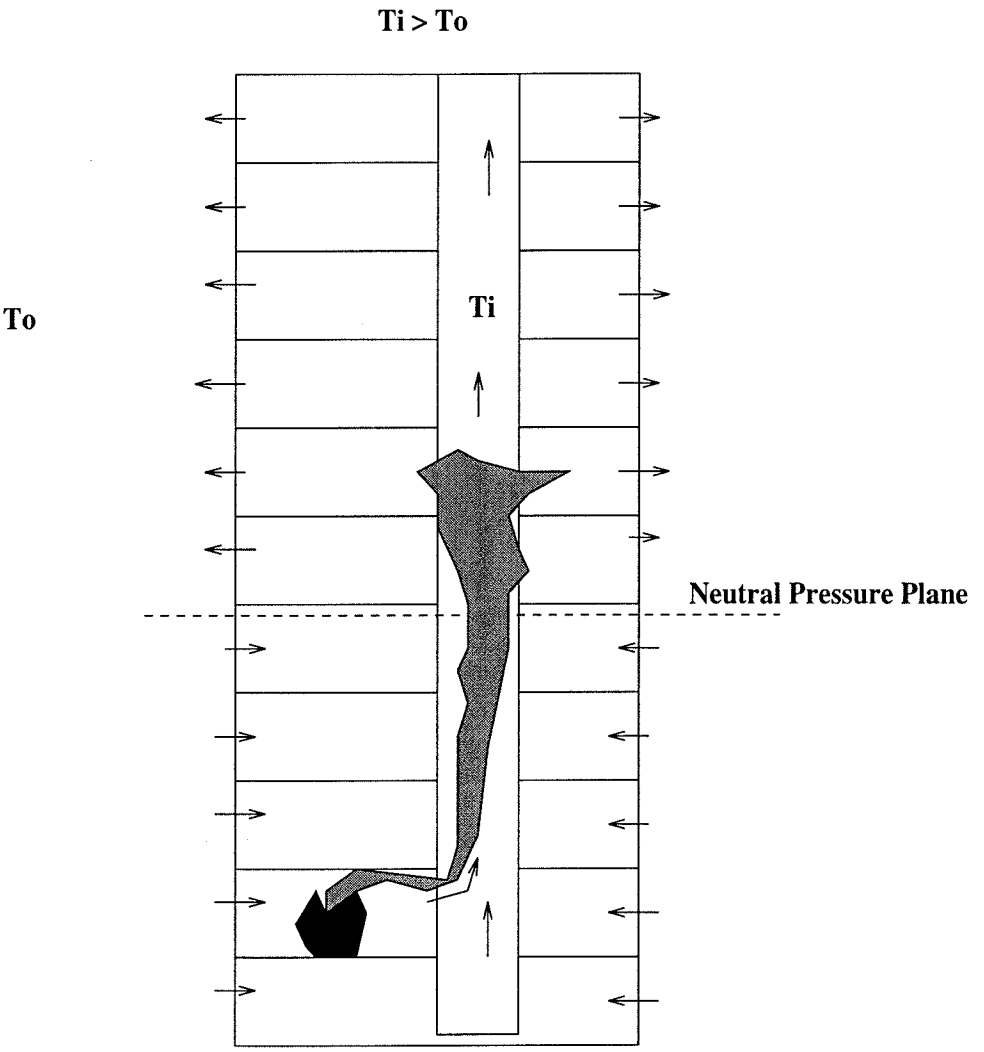

Figure 1.1: Stack effect for a tall building

for an air-conditioned building in the summer, the scenario would be reversed, i.e., smoke would tend to flow downward and out of vertical shafts, *below* the neutral plane. This is called the reverse stack effect. Mcguire and Tamura (1975) provide simple techniques for the calculation of the neutral plane location for compartments with various types of vents.

Turbulent Mixing: If toxic fumes from a fire enter a vertical shaft from the bottom, the fumes initially rise like a buoyant plume. However, as the plume grows and entrains more air, its diameter will be large enough to include the entire cross-

sectional area of the shaft. Since colder, denser gases lie above the hot plume, an unstable density stratification exists. Turbulent mixing is a result of this gravitational instability and is strongly dependent on the magnitude of the density gradient. Even though this process does not usually produce as rapid a transport of gas as the stack effect, it is always present during a fire, even if the shaft has no other openings or leaks. As the smoke travels away from the fire, its temperature drops due to heat transfer to the walls and dilution with ambient air. Thus the buoyancy of the smoke, and hence the turbulent mixing, is reduced with distance from the fire. An extensive discussion of the turbulent mixing process can be found in Zukoski (1995)

Air Handling System: The building's heating, ventilating and air-conditioning system can aid in detecting a fire in its early stages. Since the system can move smoke to undesirable locations, such as rooms occupied by people, the air circulation system often automatically stops when a fire is detected. However, even if the fans are shut off, smoke can be transported through the air handling ducts by the stack effect and turbulent mixing processes.

External Wind: If a strong wind is present during a fire, it can have an effect on the movement of smoke. The wind tends to move air from the windward side to the leeward side of the building due to the existence of small leaks or open windows. The pressure differences caused by the wind depend on its intensity and direction as well as the geometry of the building.

1.3 Background

The stack effect and turbulent mixing are the primary forces responsible for the movement of smoke and are the focus of this study. This investigation is an extension of a study by Cannon (1975), which was centered on the turbulent mixing. Cannon's work primarily involved a convective mass transfer experiment. Instead of hot air rising into denser ambient air, pure water was allowed to rise into a shaft filled with salt water. The fluids were initially separated and allowed to mix by removing a

partition at a specified time. The progress of the rising front and the subsequent mixing was monitored by measuring the concentration of salt in the tube. Cannon observed intense mixing in the shaft long after the initial front had reached the top. The study also included an analytical model in which the diffusion equation was solved. A fundamental time scale that characterizes mixing and a diffusion coefficient for the unstably stratified fluid was found. The turbulent mixing coefficient was a function of the density gradient, gravity and the length and diameter of the shaft.

The movement of smoke and hot gases in vertical shafts has also been experimentally studied by Marshall (1984) and by Mercier and Jaluria (1995). These investigations involved the introduction of hot gases from a side vent near the bottom of a vertical shaft and simulated the progression of smoke from a corridor into a vertical duct. The latter study also included schlieren flow visualization.

Extensive research has been performed on high rise fire safety systems. Tamura (1982) describes experiments performed in a 34 story office building to test a proposed smoke control system. Paul (1984) reports the results of a survey of 135 residential and office buildings in Calgary. The paper describes prevailing smoke control systems and proposed modifications to them. Buckley (1985), discusses the historical development of fire safety systems and provides suggestions for integrating smoke control with the buildings' existing air handling system.

Zone (or finite element) models are often used to approximate fires in buildings (Zukoski and Kubota, 1980; Emmons, 1983). These models simplify a complex fire by assuming that the fire and its surroundings are made up of a number of zones each with uniform properties. In the simple two layer model, the fire environment is described by an upper, higher temperature smoke layer and a lower, cooler and less buoyant ambient layer. This stratification has often been observed in real building fires. Initially the room consists entirely of the lower temperature layer. Smoke entering the room rises as a buoyant plume to the ceiling and forms the upper layer thereby lowering the interface. The two layers are gravitationally stable.

The Building and Fire Research Laboratory of the National Institute of Standards and Technology (NIST) developed a zone model called the Consolidated Fire And

Smoke Transport (CFAST) model for predicting the behavior of a multi-compartment fire. CFAST uses a two layer model for each room and is based on the conservation of mass, energy, and momentum and on the ideal gas law (Peacock et al., 1993). In the model, the fire plume that forms above any burning object is considered a means of transporting mass and energy from the lower layer to the upper layer. Mass and energy can also can be transferred across vents such as windows and doors. Given a specified fire this model calculates the distribution of smoke, toxic gases and temperature throughout the building as a function of time. Jones and Forney (1993) discuss improvements in the CFAST model.

Although zone models can often successfully simulate fires in compartments, the two layer model will not accurately approximate the behavior of smoke movement in vertical shafts with a large aspect ratio. He and Beck (1997) describe experiments in a full-scale four story building, and observed that the stack effect combined with the mixing and heat transfer processes prevented the formation of a stratified hot upper layer and cool lower layer. Cooper (1994) utilized the experimental results of Cannon and other researchers to develop a set of equations valid for tall vertical shafts. Cooper derived the turbulent diffusion coefficient as a function of the density ratio, the channel diameter and the gravitational constant for the special case of a closed shaft with no heat transfer. These results could be utilized in modeling large aspect ratio shafts in a multi-compartment fire with traditional zone modeling in the other compartments.

Fire models such as CFAST are continuously being expanded to include additional phenomena. Model developers rely on data from experiments to validate and improve fire models.

The movement of smoke in vertical channels results in either a free or mixed convection heat transfer problem. Yang (1987) and Ostrach (1988) provide comprehensive reviews of the work done on natural convection in enclosures. Brown and Gauvin (1965) performed mixed convection experiments in a vertical shaft with a circular cross section. A large number of numerical studies on mixed convection have been performed including one by Kim and Jaluria (1998) which entailed laminar flow

of hot gases in a vertical shaft.

1.4 Objectives

This study simulates smoke movement due to a fire in vertical shafts of high-rise buildings while expanding on Cannon's work. In a real fire, smoke entering a vertical shaft would first travel from its source through a connecting compartment such as a corridor after which the smoke would enter the vertical channel from an opening such as a doorway (Cannon, 1975). This study focuses on a simplified scenario where a long vertical shaft containing air at ambient conditions is suddenly exposed to a large volume of hot air as illustrated in fig. 1.2. This simplification permits a clearer definition of the boundary conditions at the bottom of the shaft while retaining the dynamics of the actual fire scenario. The experiments involved hot air rising in this vertical shaft. In some cases the shaft contained a small amount of tracer gas.

Initially, the turbulent mixing process is studied using completely closed channels. However, since the stack effect and turbulent mixing often occur concurrently during a fire, the two mechanisms are studied together utilizing vented channels. For the closed shaft flows natural convection is the primary driving force. Both natural and forced convection forces are present in the vented shaft resulting in a mixed convection experiment. The results of this work are compared to experimental studies of free and forced convection in closed channels.

The progress of the initial front of hot gas is monitored with the objective of developing scaling laws for the arrival time of the front at different parts of the shaft. The temperature, velocity, and in some cases the concentration, of the gases inside the shaft are measured as a function of time, elevation and geometrical parameters of the shaft. A heat transfer coefficient is experimentally determined by measuring the heat flux through the walls of the duct. The heat transfer is important since the removal of energy from the rising hot gas changes the dynamics of the mixing process. In addition to the experimental measurements, the study also includes a simple analytical model to validate the experimental results.

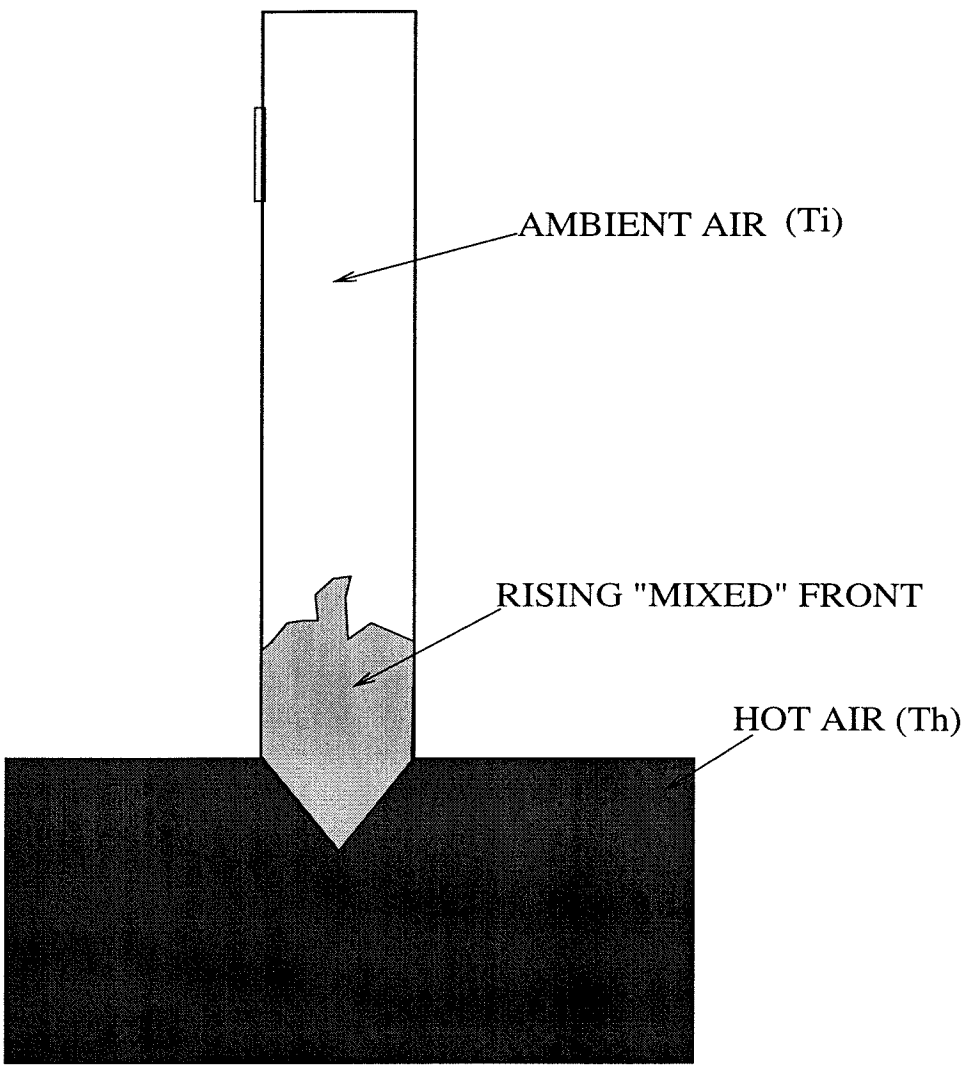

Figure 1.2: Simplified fire scenario

The remainder of this document details the experimental and analytical study of convective flows in vertical shafts. Chapter 2 describes the small scale experimental apparatus and the experimental procedure. The measurements with thermocouples and heat flux gauges are outlined. The constant temperature hot wire anemometer system employed to measure the flow velocity and the gas analyzer utilized to measure the concentration of a tracer gas are described. The chapter also contains a description of the data acquisition system. In Chapter 3, the results of the natural convection experiments in closed channels that simulated turbulent mixing alone are presented and discussed. Chapter 4 is a description of the mixed convection experiments in vented channels, which combine the stack effect and turbulent mixing. Chapter 5 explains the analytical model that is based on a simple instability analysis and an energy balance. The summary and conclusions of this investigation are found in chapter 6.

Chapter 2 Experimental Apparatus and Procedure

2.1 Test Setup

The 1/12 scale experiment was designed to investigate the movement of hot fire products in a high-rise building. The experiments were performed in a 2.59 m tall vertical shaft with a square cross-section. Two shaft sizes, 15.24 cm x 15.24 cm and 25.4 cm x 25.4 cm, were used resulting in aspect ratios, $H/w = 17$ and $H/w = 10.2$ respectively, where H is the height of the shaft and w is the width. Completely closed shafts were employed to study the effect of turbulent mixing only, while shafts with openings were used to examine the stack effect and turbulent mixing together.

2.1.1 Closed Channel Experiments

Two classes of experiments were performed in closed shafts. In one, the vertical shaft initially contained air at room temperature. In the second, the shaft was filled with a mixture of carbon dioxide and air. A schematic for the single component experiments is shown in fig. 2.1. The vertical shaft was situated above a large cylindrical reservoir. The walls of the shaft were 1.27 cm thick aluminum. The reservoir was 0.91 m tall and 1.22 m in diameter, and was separated from the shaft by a brass sliding partition. This partition contained small channels for water cooling.

The reservoir was filled with hot air before the start of the experiment. The heating was accomplished by resistive heating elements contained in a chamber and a blower with a maximum flow rate of 0.17 m^3/s. The four heating elements had a total power output of about 6800W and were rated for 540°C. Room temperature air was sent through the blower and over the heating elements into the reservoir. Air

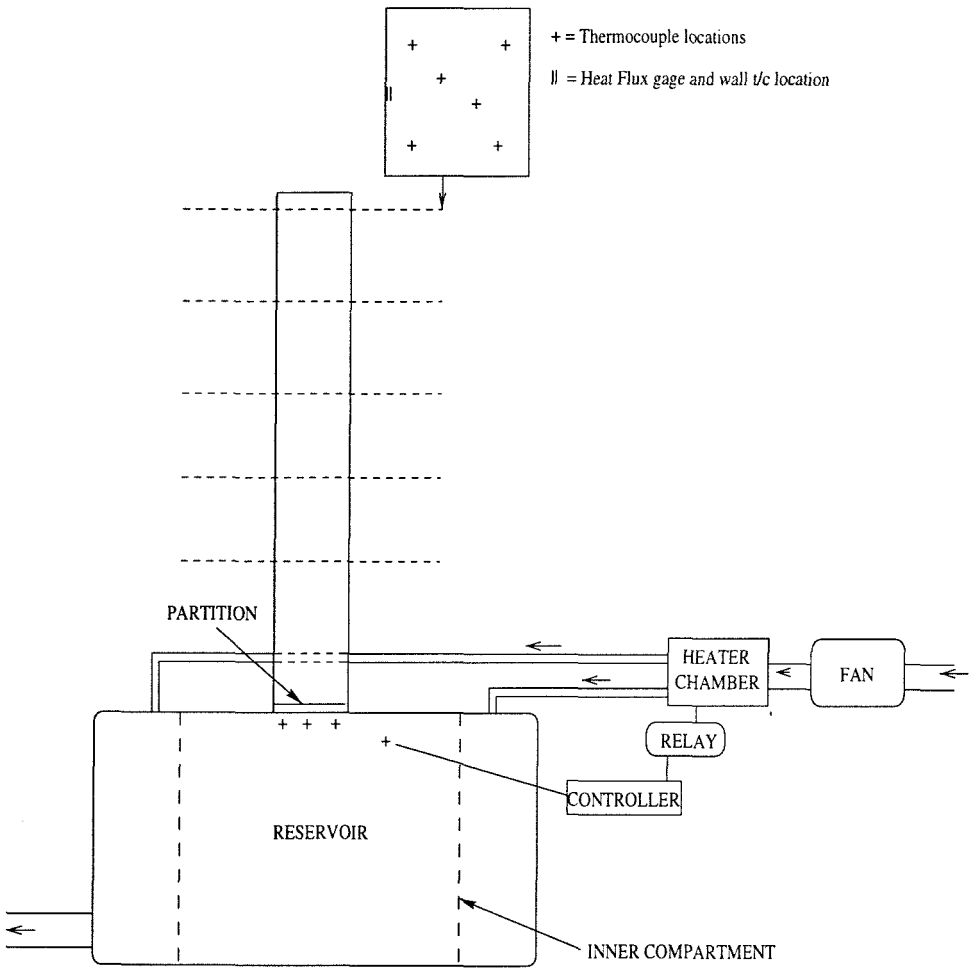

Figure 2.1: Experimental setup: Closed channel

from the heaters was introduced to the reservoir at four different points to provide even heating. The hot air leaving the reservoir was exhausted to the atmosphere. The hot gas reservoir and the heater chamber were covered with insulator blankets to minimize losses.

Since turbulent mixing is a process driven by natural convection, it was important to mitigate forced convection effects due to the blower. For this purpose the reservoir was comprised of two compartments as seen in fig. 2.1 with the walls of the inner chamber consisting of numerous small orifices. The heated air initially entered the outer compartment and was convected into the inner container.

The reservoir temperature was monitored by a microprocessor based, auto-tuning controller and a solid state relay. A K-Type thermocouple placed in the reservoir was the input to the controller. When the blower and heater were turned on, the controller was set to the desired reservoir temperature. The output of the controller was connected to the solid state relay that switched power on and off to the heaters. The time taken for the reservoir to reach the pre-determined temperature varied from 25 to 60 minutes. Once the desired temperature was reached, the partition separating the reservoir from the vertical channel above was opened in a swift horizontal motion, and the hot air inside was allowed to mix with ambient air in the shaft. Before the partition was opened, the initial conditions in the shaft were monitored for 60 seconds. After opening the gate, the conditions were recorded for a further 20 minutes. The reservoir temperature was held constant to within $\pm 1^{o}$C for the course of an experiment. Different trials were conducted by varying the reservoir temperature from 80 to 120^{o}C.

Two sizes of shafts were used in the study. The larger 25.4 cm shaft was modified with inserts to make the smaller shaft as shown in fig. 2.2. Two of the four sides of the channel had removable plates, each about 48 cm in length. On one side of the shaft these plates were used to mount the instrumentation while the other side was used to access the shaft. Once a shaft was assembled, it was sealed to be as leak free as possible. The temperature of the gas and wall and the heat flow-rate through the wall were determined at various elevations.

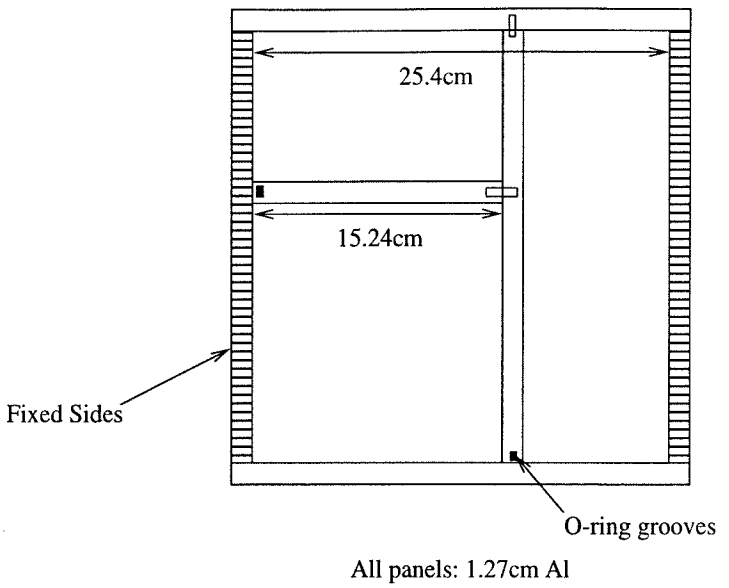

Figure 2.2: Plan view of vertical channel

The two component experiments used a trace amount of CO_2 in the vertical shaft. Figure 2.3 shows the instrumentation for these experiments. The shaft was initially filled with a calibrated mixture of air and 5% CO_2 from the gas bottle. Approximately 15 minutes later the gas bottle was shut off and a small pump was turned on for a period of five minutes to create a uniform concentration of the tracer species in the shaft. Then the concentration of the CO_2 tracer gas was measured at either, two or three elevations. The procedure was repeated until the concentration was uniform within 2.5% at the different locations and the CO_2 concentration was 4.00 $\pm$ 0.20 percent by volume. Subsequently the hot reservoir air was allowed to rise into the ambient air containing the tracer species. The procedure was the same as in the single component experiments. In three of the tests, however, the mixing was allowed to occur without any heat transfer, i.e., with no initial temperature gradient. However, since the CO_2 is heavier than air, the density gradient was non zero, although smaller than the gradients produced with the heated reservoir. The concentration of CO_2 was measured by a gas analyzer. These experiments were all carried out in the 25.4 cm duct.

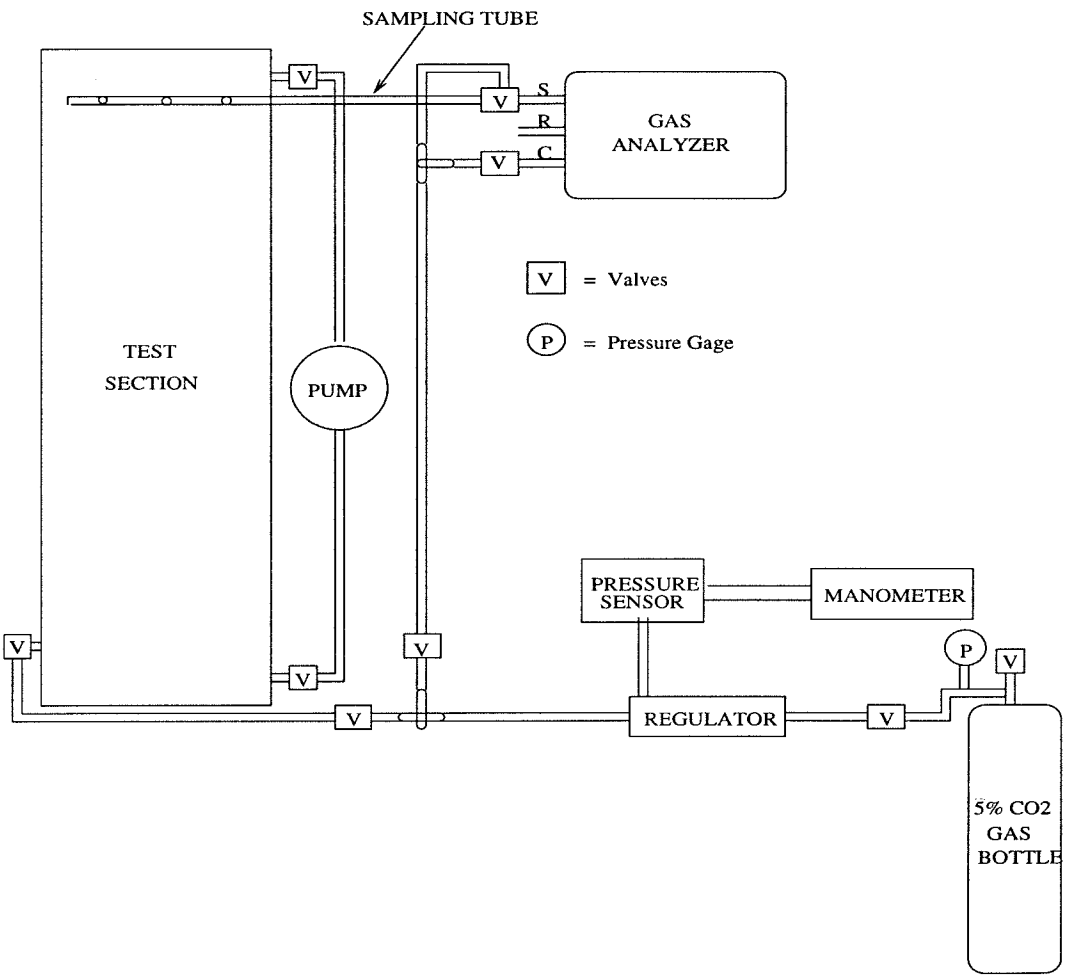

Figure 2.3: Setup for tracer gas experiments

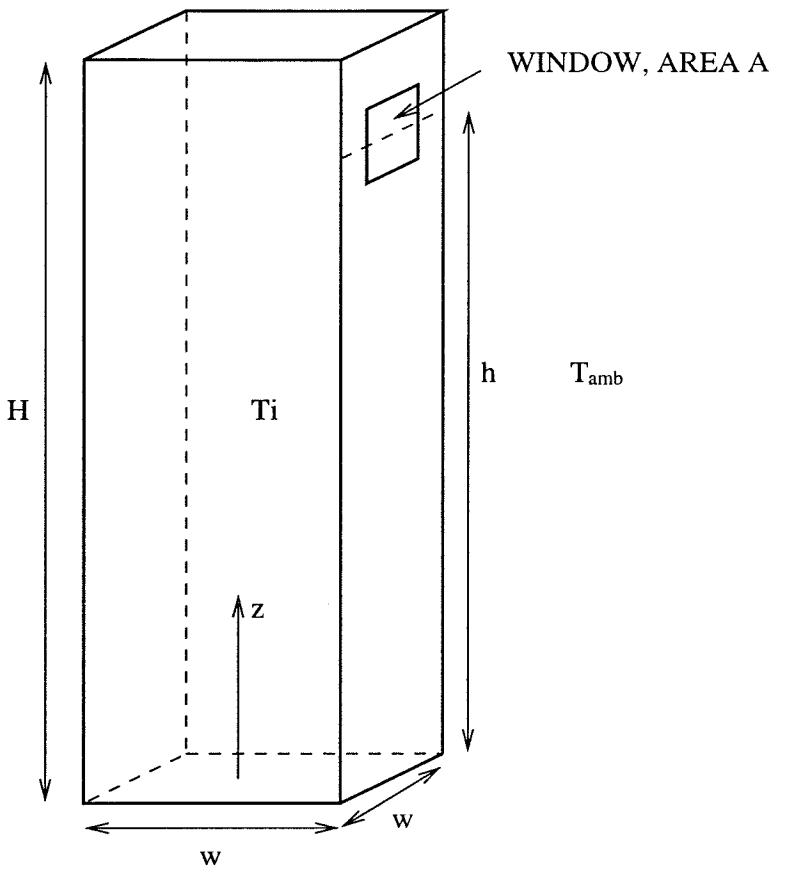

Figure 2.4: Dimensions for vented channel

2.1.2 Vented Channel Experiments

The stack effect is an important factor in the movement of smoke during a fire and is discussed in chapter 1. It was attempted to reproduce the stack effect in 30 m tall square shaft in a high rise building in the 2.59 m tall vertical shaft in this investigation. A simple analysis using the Bernoulli equation was used neglecting effects of viscosity and heat transfer (see Zukoski 1995). A schematic of shaft along with dimensions is shown in fig. 2.4.

For the full scale shaft assuming $H = 30.6$ m and $w = 3$ m gives $H/w = 10.2$. Consider a square window with dimensions, 1.2 m x 1.2 m (area, $A = 1.44$ m^2) located at $z/H = 0.95$. Thus $A/w^2 = 0.16$ and $h/H = 0.95$. From equation (1.3), the pressure difference across the window due to the stack effect is $\Delta\rho gh$, where $\Delta\rho = \rho_{amb} - \rho_i(h)$.

Thus from Bernoulli's equation, the velocity of the air out of the vent is

$$V = \sqrt{2\frac{\Delta\rho}{\rho_i(h)}gh} \tag{2.1}$$

The volumetric flow rate, $Q = AV$. Hence, the residence time in the shaft is

$$t_{res} = Hw^2/Q \tag{2.2}$$

since Hw^2 is the volume of the channel. A non-dimensional residence time can then be defined as

$$\tau_{res} = t_{res}\sqrt{g/h}. \tag{2.3}$$

For the full scale building, assume T_{amb} = -5°C and $T_i(h)$ = 22°C. Therefore $\Delta\rho/\rho_i(h) \approx 0.1$. Equations (2.1)-(2.3) then give V = 7.55 m/s, t_{res} = 25.3 s and, τ_{res} = 14.7.

For the vertical channel in this study, when w = 25.4 cm, H/w = 10.2. In order to obtain the same A/w^2 as the full scale model, a square vent of area A = 0.01 m^2 was made in the shaft at z/H = 0.95. In this case T_{amb} = 22 °C and assuming $T_i(h) \approx$ 50°C, once again, $\Delta\rho/\rho_i(h) \approx 0.1$. This gives, V = 2.19 m/s, and Q = 0.023 m^3/s (46 CFM). Thus, t_{res} = 7.37 s and, τ_{res} = 14.7.

The existing experimental setup for the closed shaft experiments was used with a few modifications as shown in fig. 2.5. An opening of area A, (A/w^2 = 0.16) was made in one of the removable plates. Two sets of experiments were conducted for the 25.4 cm shaft with the opening at elevations, z/H = 0.70 and 0.95. Only one set of experiments were conducted for the smaller 15.4 cm shaft with the opening at z/H = 0.95. The air was withdrawn from the aperture at externally controlled rates. The withdrawal mechanism consisted of a blower, a ball valve and a laminar flow element (LFE). From the analysis above a flow rate of 46 CFM was required through the vent. The 1/2 Hp (186 W) blower was selected based on the flow-rate required and the total pressure loss in the venting system.

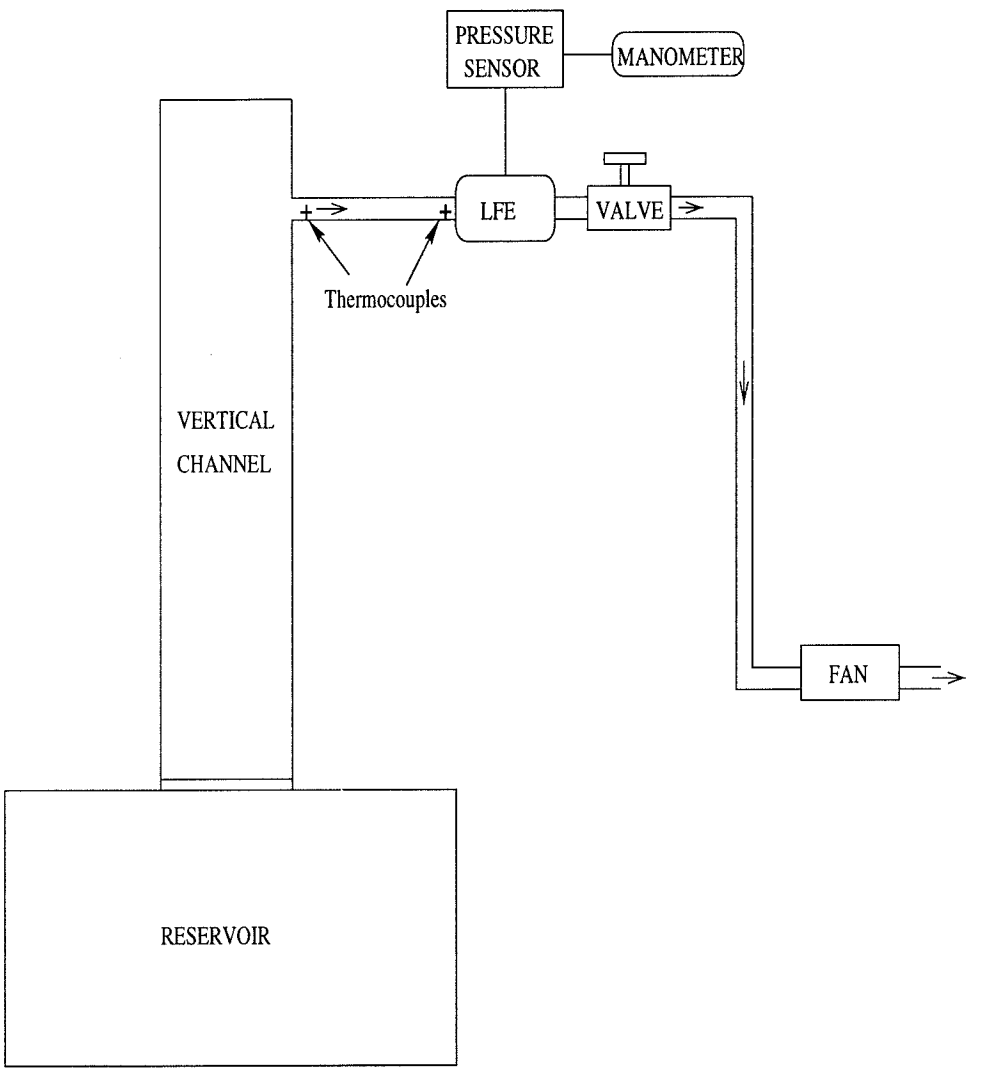

Figure 2.5: Vented shaft flow withdrawal system

For all the vented shaft experiments the reservoir was held at 100°C. The procedure was the same as for the closed shaft, except that the venting fan was turned on at the same instant that the gate was opened. The duration of the experiments was 21 minutes. The laminar flow element measured the volumetric flow rate (Q) for each experiment. The temperature of the gas entering the LFE was also measured. The mass flow rate ($\dot{m}$) is then given by $\dot{m} = \rho_{lfe}Q$ where ρ_{lfe} is the density of the gas entering the LFE. This mass flow rate was constant for the duration of a given experiment.

2.2 Temperature and Heat Transfer Measurement

The gas temperature was measured using Type-K (Chromel-Alumel) thermocouples manufactured by Omega Engineering. These 0.05mm, fine wire thermocouples were soldered onto 1.6 mm stainless steel sheathed Omegaclad wire as shown in fig. 2.6. Magnesium oxide insulation in the core separated the two legs of the thermocouple. The omegaclad wire was then connected to other extension wire outside the shaft. The thermocouples, which had a sensitivity of 40 $\mu V/^oC$ and a response time of 0.20 s in quiescent air (Omega Engineering Inc., 1992), were mounted at five different elevations in the channel; z/H = 0.23, 0.42, 0.61, 0.79, 0.98. There were six thermocouples at each cross section. Additionally, the reservoir temperature was also measured using thermocouples. The probes were calibrated using both an ice bath and boiling water.

The heat flux through the wall of the duct was measured by micro-foil heat flow sensors manufactured by RDF. The sensor is essentially a thin foil consisting of "thermal barrier" of thickness s, and thermal conductivity k. Two thermocouples measure the temperature on either side of the barrier. If the temperature difference is ΔT, the rate of heat flux through the foil is given by $Q = (k/s)\Delta T$. The sensors had a sensitivity of about 2.0 μ V/(W/m^2) and a response time of 0.70 s. The sensors were adhered to the inner walls of the duct with a high thermal conductivity silicone grease. The gauges also measured the temperature of the wall. One or two of these heat flux gauges were located at each of the five vertical locations mentioned above.

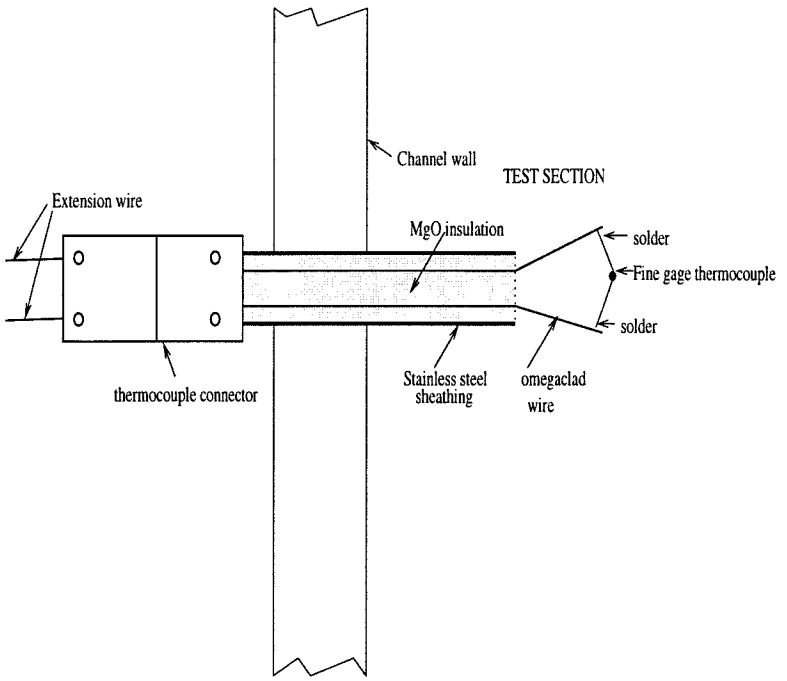

Figure 2.6: Thermocouple construction

A hot plate with a known electrical output was employed to calibrate the heat flow sensors.

2.3 Velocity Measurements

The velocity measurements were conducted with the aid of a Dantec constant temperature anemometer (CTA) system. The measuring equipment consisted of a 56C01 CTA, and the 56C17 CTA bridge, mounted on a 56B12 main frame. A type 55P11 single sensor hot wire probe is mounted on a probe holder and connected through a BNC cable to the bridge. Each CTA/bridge combination was capable of measuring a single directional component of the flow velocity and functioned as plug-in modules to the main frame. Shih (1994) has a more detailed description of the CTA system.

The probe sensor forms one arm of a Wheatstone bridge. The bridge is initially balanced when the probe is heated to its usual operating temperature (T_s) in still air. This operating temperature is usually determined from the overheat ratio of the

probe given by $a_R = (R_s - R_0)/R_0$. Here R_0 is the sensor cold resistance at flow temperature and R_s is the resistance of the sensor at T_s. The overheat ratio for this study was chosen as 80% which resulted in a sensor temperature of approximately 245°C. When the flow velocity is increased so is the heat loss from the sensor. This causes a temperature change in the sensor and an unbalance to the bridge. A servo-amplifier restores the temperature to its original value and changes the output voltage. This voltage is then a measure of the flow velocity.

If the heat transfer from the sensor wire to the fluid is assumed to be primarily by forced convection, the hot wire voltage (V) is given by

$$\frac{V^2}{R_s} = h(T_s - T_o) \tag{2.4}$$

where h is the heat transfer coefficient and is a function of the flow velocity (u). Often a relationship of the form

$$h = a_1 u^n + a_2 \tag{2.5}$$

is assumed (Bruun, 1995). Here $n \approx 0.5$ and a_1 and a_2 are constants determined by calibration.

The probes were calibrated using an experimental airjet facility consisting of a blower and nozzle (see fig. 2.7). When the blower was turned on, the air issued from the nozzle at a rate that could be controlled by a valve. The hot wire probe was placed about 3 cm from the nozzle exit at the centerline of the flow and the output voltage (V) was recorded. A Pitot tube was then placed at the same position and the dynamic pressure (P_d) was measured using a manometer. Since the dynamic pressure is related to the velocity by $P_d = 1/2\rho u^2$, the velocity u was thus determined. The process was repeated at six different flow-rates.

These calibration trials were conducted at room temperature with a fixed 80% overheat for the CTA bridge. Thus R_s, T_s and T_0 are constant. Therefore, from (2.4) and (2.5), the relationship between the velocity and voltage is $u^{1/2} = b_1 V^2 + b_2$, where b_1 and b_2 are constants. Thus a plot of $u^{1/2}$ versus V^2 gives a straight line and the

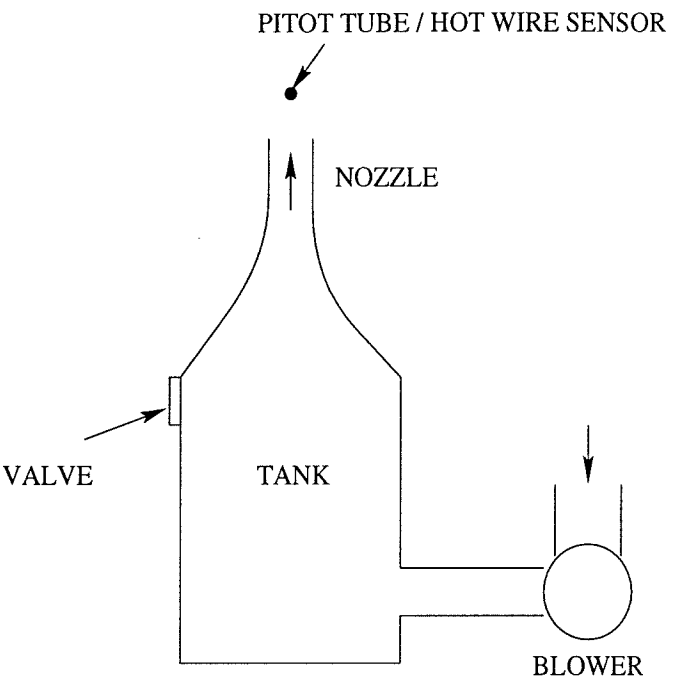

Figure 2.7: Air jet facility for calibrating anemometers

velocity is obtained by

$$u = (b_1 V^2 + b_2)^2 \tag{2.6}$$

This calibration does not account for changes in flow temperature that occured in most of the experiments in this study. A change in flow temperature causes the overheat ratio to change and thereby modifies the voltage output. Equation (2.4) implies that the voltage output is related to the flow temperature T as, $V^2 \propto (T_s - T)$. Lemieux and Oosthuizen (1985) investigated the impact of varying fluid temperature on the output voltage of the hot wire. They obtained a relationship of the form, $V^2 = (a_1^* u^n + a_2^*)(T_s - T)$, for $20^o C < T < 60^o$C.

The airjet facility was modified to verify the results of Lemieux et al. A hair dryer was placed at the input to the tank and Pitot tube, and hot wire measurements were taken at the nozzle exit for two heat settings and two flow settings. It was observed that the square of the hot wire output voltage decreased linearly with increasing flow temperature at a contant flow-rate for temperatures up to 65^oC. Given a CTA output

voltage V_{obs} at the flow temperature, $T > T_o$, the corrected output voltage can be then obtained from

$$V^2 = \frac{(V_{obs})^2(T_s - T_0)}{(T_s - T)} \tag{2.7}$$

The velocity is then given by equation (2.6)

The hot-wire measurements were taken at an elevation of $z/H = 0.40$ in the larger 25.4 cm shaft for both closed and vented flows. The probe was placed on a horizontal traverse and measurements were taken at various distances from the wall to obtain a velocity profile. Temperature readings were also simultaneously procured so that the output voltage could be corrected for changes in flow temperature.

2.4 Concentration Measurements

For the experiments that used a tracer gas, a 20 series gas analyzer manufactured by Gow-Mac measured the concentration of CO_2 in the channel (see fig. 2.3). The analyzer unit consisted of three input lines (Sample, Reference, and Calibration), a pump, a 10-077 thermal conductivity detector (TCD), an analog readout meter and and circuitry to provide an electronic output. The analyzer had a range of 0 - 5% CO_2 and an accuracy of 0.5%.

The internal pump brings in the sample and reference gases (or the calibration and reference gases) to the analyzer. The TCD has an electrically heated hot element as a branch of a Wheatstone bridge circuit. The sample gas was then fed through a cavity containing this heating element. A constant current flows through the element resulting in a constant rate of heat dissipation. If the concentration of the sample gas changes, so does the thermal conductivity, and hence a different temperature difference between the sample gas and element are required to maintain the same heat dissipation. Therefore, the temperature of the hot element changes, changing its resistance which is measured by the Wheatstone bridge circuit.

The analyzer was calibrated before each experiment. The contents from the gas bottle were fed through the calibrate input line of the analyzer, and lab air was

supplied through the reference input line. Since the concentration of CO_2 in the gas bottle was known, the output of the analyzer could be adjusted. During the experiment the analyzer sampled gas from the vertical shaft at 60 cc/min. Since this resulted in only removing 0.8% by volume of the channel for the entire experiment, the sampled gas was not returned to the channel. For a given experiment the analyzer sampled from one of three vertical locations: $z/H = 0.23$, 0.61 or 0.98.

The response time of the analyzer was about 4 seconds, but the presence of the long sampling tube from the test section to the analyzer resulted in increasing the response time to 30 s. The temperature of hottest gases entering the sampling tube was about 70°C. However, since the flow in the sampling tube was laminar and the diameter of the tube was small, the highest temperature of gas entering the analyzer was only 0.5°C above ambient and hence no cooling was required for the sampling gas.

2.5 Flow-Rate Measurements

For the vented shaft experiments, the withdrawal flow-rate was measured by a laminar flow element. The laminar flow element (LFE) is a tube made up of an array of very fine channels, small enough to ensure laminar fully developed flow through them (Fox and McDonald, 1985). The volumetric flow-rate through the flow element $Q \propto \mu dP/dx$ where dP/dx is the pressure gradient in the direction of the flow and μ is the dynamic viscosity of the fluid. Since the viscosity is function of temperature, the flow-rate can be determined by measuring the pressure drop across the LFE and the temperature of the air entering the LFE. The pressure drop was evaluated by a pressure sensor and electronic manometer. A thermocouple measured the temperature at the LFE inlet. The flow element had a linear output up to 50 CFM (23,600 cm^3/s) and had a pressure drop of 4 inches of water (998 Pa) across it at the highest flow-rate. A valve downstream of the LFE was used to adjust the flow-rate. However, each experiment was conducted at a constant withdrawal rate and a range from 4700 to 19,000 cm^3/s was examined.

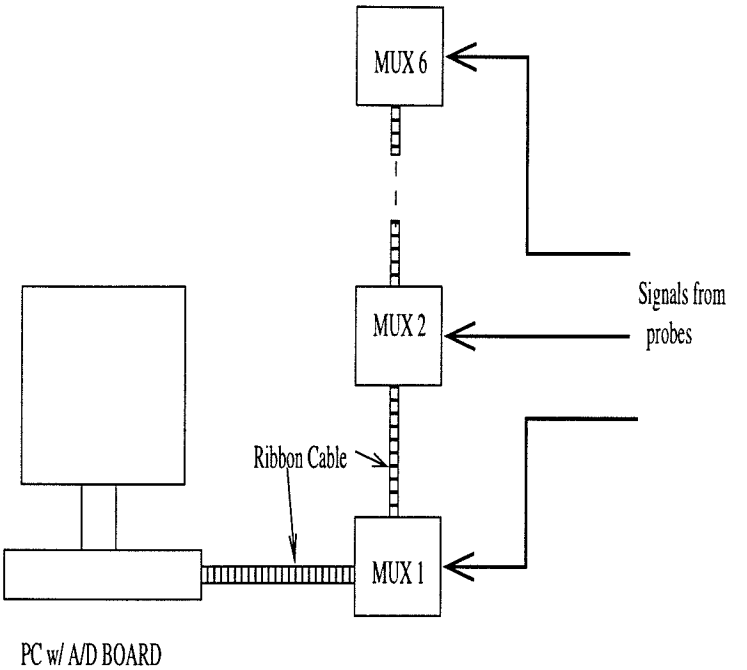

Figure 2.8: Data Acquisition System

2.6 Flow Visualization

A simple flow visualization study with smoke wire was performed for the closed channel. The procedure is detailed in Appendix B.

2.7 Data Acquisition

A data acquisition system (fig. 2.8) was used to simplify data gathering and analysis.

Signals from the probes and the gas analyzer were sent through a multiplexer and into a data acquisition board. A 90 MHz personal computer with a Pentium processor was utilized for data acquisition. The DAS-20 data acquisition board from Keithley Metrabyte performed the analog to digital (A/D) conversions of the signals. The A/D board had a resolution of 12 bits and eight differential input channels. The maximum possible input to the DAS-20 board was $\pm$ 10 volts.

The mutiplexers, which were type EXP-20, enabled each DAS-20 channel to be

expanded to 16 differential channels. Up to six multiplexers were used for a given experiment. The mutiplexers were equipped with amplifiers and low pass filters for signal conditioning. The amplifier gain could be set by a dip switch from a range of 1 to 800. A gain of 800 was selected limiting the largest input signal to the EXP-20 to be $\pm$ 12.5 mV. Therefore, the maximum temperature that could be read by the combined DAS-20/ EXP-20 data acquisition system was about 300^{o}C. The multiplexers also had built-in cold junction compensation for thermocouples. The sampling rate was 10 Hz for the tests that involved velocity measurements while it was 3 Hz for all of the other experiments.

Chapter 3 Experimental Results: Closed Channel

The experimental facility consisted of a reservoir and a vertical channel initially separated by a partition. The reservoir was filled with heated air while the channel contained ambient air. For some experiments a small amount of carbon dioxide was added to the vertical channel as a tracer gas. As the partition was removed the hot air rose into the vertical shaft. The progress of the initial front of hot gas was monitored by measuring the temperature at various locations in the shaft. An initial transient period of lasting less than two minutes was seen until after the initial front reached the top of the shaft. Thereafter, a pseudo steady state situation prevailed in the channel.

3.1 Transient State

3.1.1 Single Component Experiments

Figure 3.1 shows a typical case of the cross-section averaged gas temperature rise for the smaller shaft plotted versus time for a 50 second duration, beginning just prior to the opening of the gate. Due to noise from the multiplexers and the data acquisition board, there were small temperature fluctuations, usually not more than $\pm 1^{o}$C, present throughout the experiment. The arrival time of a front was defined as the time at which the mean temperature rise at a cross section was 25 % greater than the highest temperature rise observed, due to noise, in the first 60 seconds.

A sharp jump in the temperature generally indicated the arrival of a front. From the graph and data for the experiment shown, the initial front reaches a location four shaft widths from the bottom in about 3 seconds, and 17 shaft widths (the top wall)

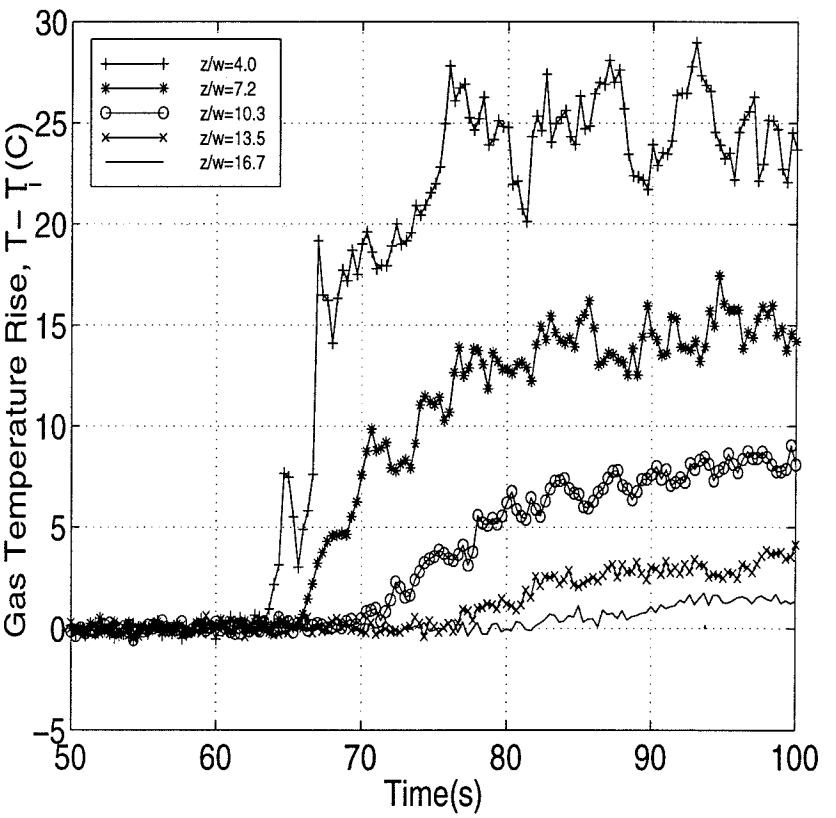

Figure 3.1: Transient measurements of average temperature as a function of time for the closed shaft with H/w =17 and for the reservoir temperature = 100^{o}C

in about 24 seconds.

However, examination of a given cross section of the duct in detail (see fig. 3.2) shows that, a temperature rise was not seen in all thermocouples at the same instant. The figure shows that the temperature profile at a cross section in the channel at a height $z/w = 7.2$, shortly after the partition was removed. In fig. 3.2(a) the front has not reached the location being observed. In the next "'snapshot", taken one second later, the temperature at $y/w = 0.6$ and 0.8 has changed significantly from its initial value, but the the temperature on the left side of the shaft has not changed. In fig. 3.2 (c) which illustrates the situation 7.33 seconds after the partition is opened, the temperature on the left side of the shaft is higher. The wall temperature was not more than 0.1 ^{0}C above ambient at the time shown, although the wall does get hotter with time. These results imply that for this trial the first front to arrive at $z/w = 7.2$ came up on the right side of the shaft, while a second front followed shortly thereafter on the left side of the shaft. This behavior was typical at any cross section and for any reservoir temperature. The initial front rose on either side of the shaft. Cannon (1975) also observed similar phenomena in his water/salt water experiments.

As expected the hotter the temperature of the reservoir the faster the hot gases reached the top of the shaft. If T_h is the reservoir temperature and T_i is the initial temperature in the shaft, and ρ_h and ρ_i are the corresponding densities, the quantity $\Delta\rho_i/\rho_{avg}$ was used to scale the arrival time for different reservoir temperatures. Here,

$$\frac{\Delta\rho_i}{\rho_{avg}} = \frac{\rho_i - \rho_h}{0.5(\rho_i + \rho_h)} = \frac{T_h - T_i}{0.5(T_h + T_i)} \tag{3.1}$$

since,

$$\frac{\rho_i}{\rho_h} = \frac{T_h}{T_i} \tag{3.2}$$

from the ideal gas law.

The location of the initial front (z_f) was expected to be a function of the density ratio, the channel width, gravity and time, i.e., $z_f = c_f(\Delta\rho_i/\rho_{avg})^{a_1} g^{a_2} w^{a_3} t^{a_4}$. Here $c_f, a_i (i = 1 - 4)$ are constants. Since $(\Delta\rho_i/\rho_{avg})g$ is the effective gravitational acceleration (Fischer et al., 1979), and an indication of the initial buoyancy

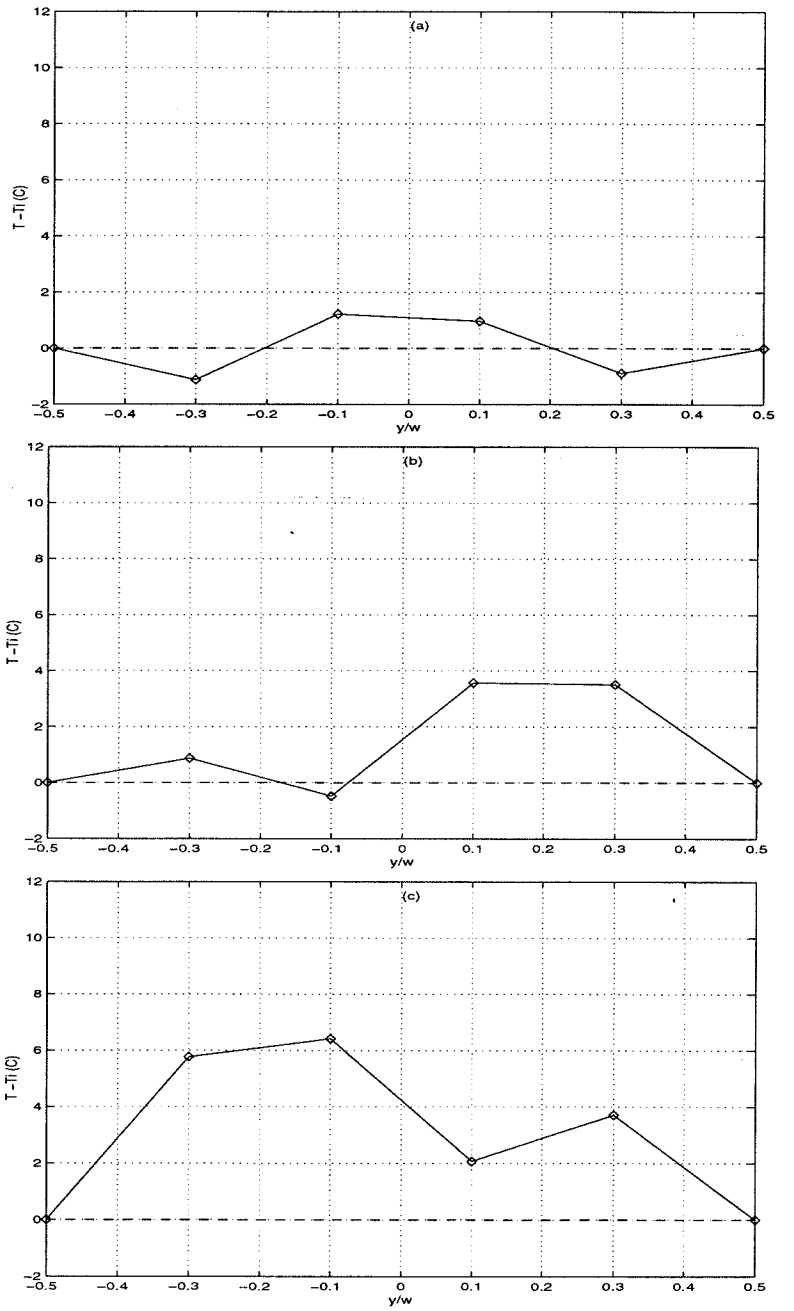

Figure 3.2: Temperature of rising front versus transverse coordinate at z/w = 7.2 at times (a) t = 5.33 s, (b) t = 6.33 s, (c) t = 7.33 s for the $H/w = 17$ shaft

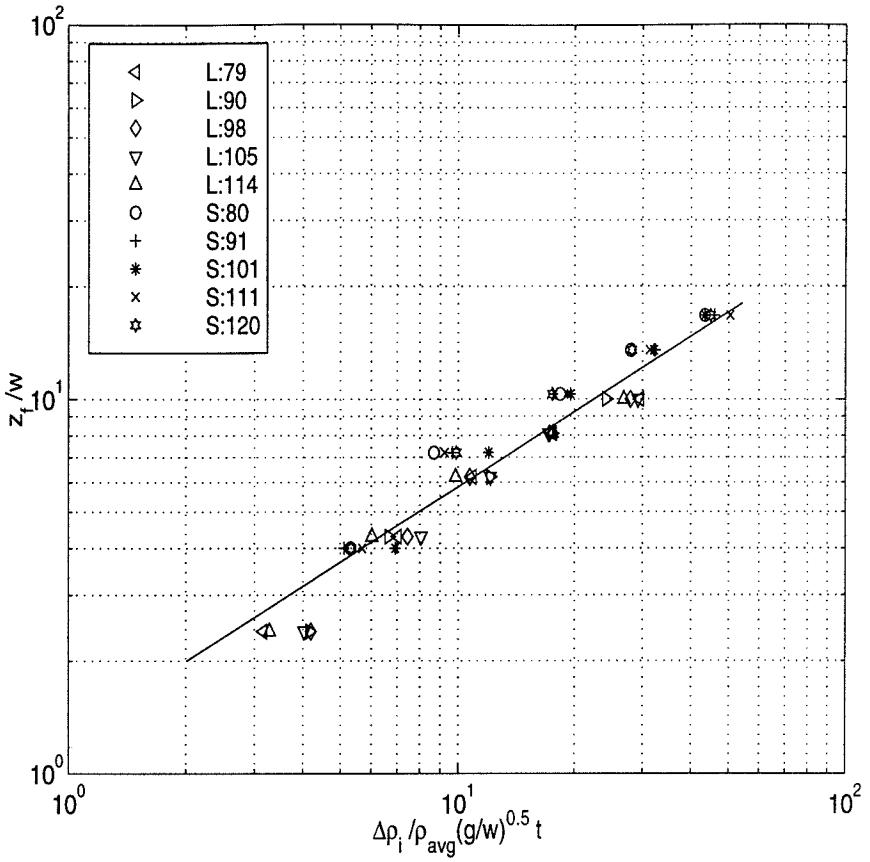

Figure 3.3: Progress of initial front versus time in closed channels. L: 25.4 cm channel and S: 15.24 cm channel at various reservoir temperatures (^{o}C)

in the shaft, $(\Delta\rho_i/\rho_{avg})$ and g were expected to appear as one term in the equation, or $a_1 = a_2$. Therefore, from dimensional analysis, a relationship of the form, $z_f/w = c_f[\sqrt{(\Delta\rho_i/\rho_{avg}(g/w))}\,t]^a$, where a is a constant, was anticipated. However, the results of this study correlated best with $(\Delta\rho_i/\rho_{avg})\sqrt{g/w}\,t$. The location of the initial front, normalized by the channel width, for the two channels examined are displayed in Fig. 3.3. The uncertainty for the front location is $z_f/w = \pm 0.05$. The heated trials investigated the range $0.172 < \Delta\rho_i/\rho_{avg} < 0.282$

The correlation shown by the solid line in the figure is given by the following expression

$$\frac{z_f}{w} = 1.41[\frac{\Delta\rho_i}{\rho_{avg}}\sqrt{\frac{g}{w}}\,t]^{2/3} \tag{3.3}$$

The arrival times at the lower part of the shafts were probably influenced by the gate opening process and the values are less accurate. Cannon (1975) obtained the relationship

$$\frac{z_f}{w} = 0.97[\sqrt{\frac{\Delta\rho_i}{\rho_{avg}}\frac{g}{w}}\, t]^{0.57} \tag{3.4}$$

3.1.2 Adiabatic Experiments with Tracer Gas

A series of tests were conducted with the reservoir at room temperature. These experiments thereby involved no heat transfer. A density difference was achieved by filling the vertical shaft with a gas mixture containing 4 % carbon dioxide and 96% air that was marginally heavier than the ambient air in the reservoir. Three experiments were conducted in the larger channel with the gas analyzer at z/w = 2.4, 6.2 and 10. When the lighter reservoir gases reach the sampling probe, the analyzer detects a decrease in the carbon dioxide concentration. The position of the initial front is displayed as a function of time in fig. 3.4. The figure also shows the front location as predicted by Cannon's correlation (equation 3.4) and by the correlation obtained in this study for the single component experiments with a hot reservoir (equation 3.3).

Both correlations under-estimate the front propagation rate though Cannon's correlation does come closer to predicting the actual location of the front. This discrepancy may be due to the heat transfer. As the front of hot air moves up the shaft, its buoyancy is changed as heat is transferred to the walls. Furthermore, the salt water experiments dealt with density differences in the range $0.056 < \Delta\rho_i/\rho_{avg} < 0.173$, which are smaller than those obtained with the hot reservoir in this study. However, the density ratio for the adiabatic experiments was only 0.021.

3.1.3 Heated Reservoir Experiments with Tracer Gas

Some experiments were performed with a heated reservoir and tracer gas in the vertical shaft. The partition separating the reservoir and channel is removed to let hot air rise into the shaft. The temperature and the CO_2 concentration was monitored

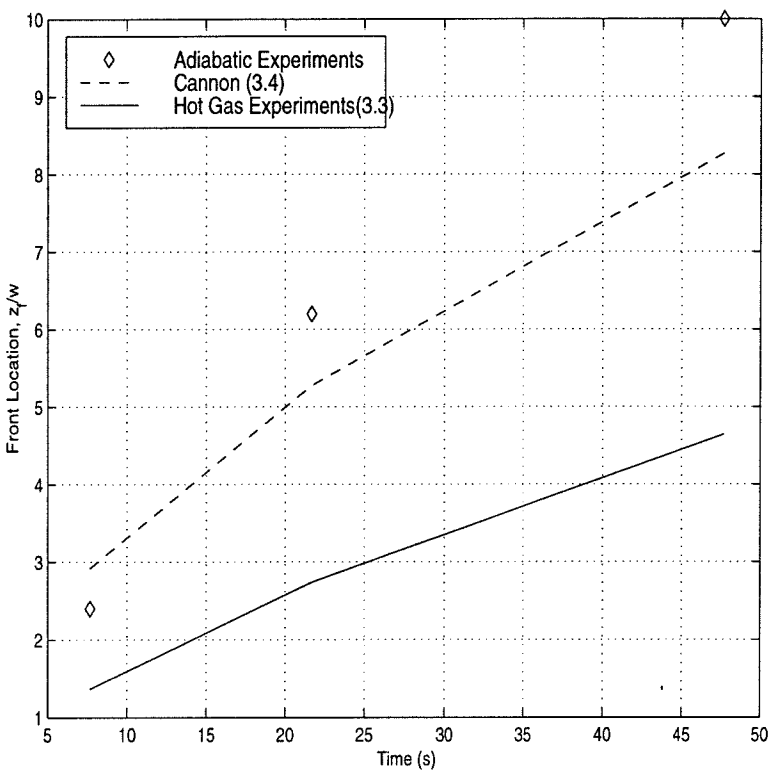

Figure 3.4: Initial front location versus time for adiabatic experiments with tracer gas. Predictions from Cannon's mass transfer experiments and the hot gas trials for the same density ratio are also shown

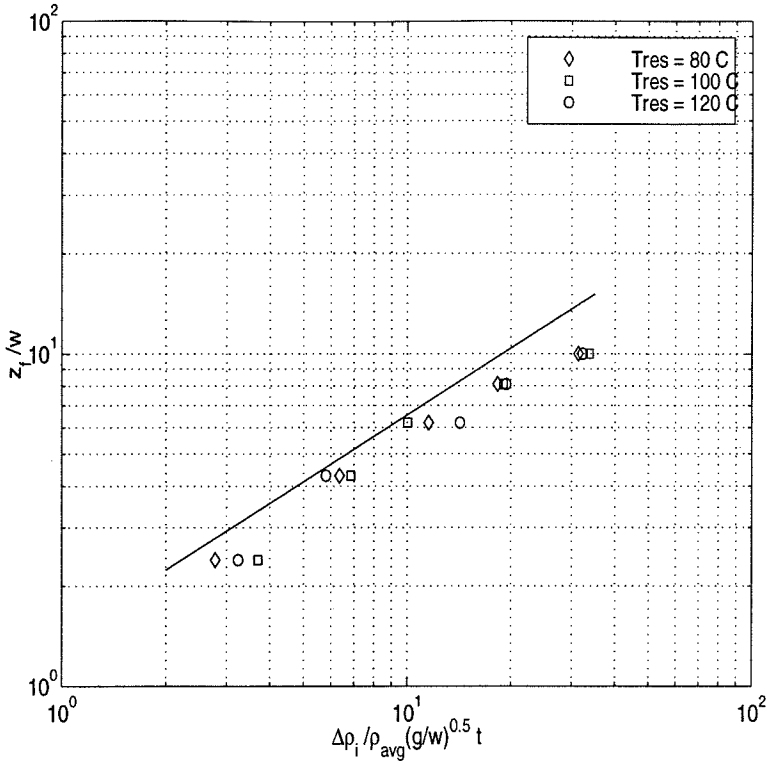

Figure 3.5: Progress of initial front versus time for the 25.4 cm channel with tracer gas at various reservoir temperatures

as a function of time and position. Fig. 3.5 shows the initial front position plotted versus normalized time for the tracer gas trials. The solid line in the figure shows the correlation obtained by the single component experiments (given by equation (3.4)). This correlation slightly overpredicts the front propagation speed for the tracer gas tests.

The concentration (C) is normalized by,

$$C^* = \frac{C - C_f}{C_i - C_f} \tag{3.5}$$

where C_i and C_f are the initial and final concentrations of CO_2. Typically $C_i \approx 4.00$ % and $C_f \approx 0.00$ % by volume.

The normalized concentration of CO_2 as a function of time for three vertical locations are displayed in fig. 3.6. Once again the partition is removed at $t = 60$ s.

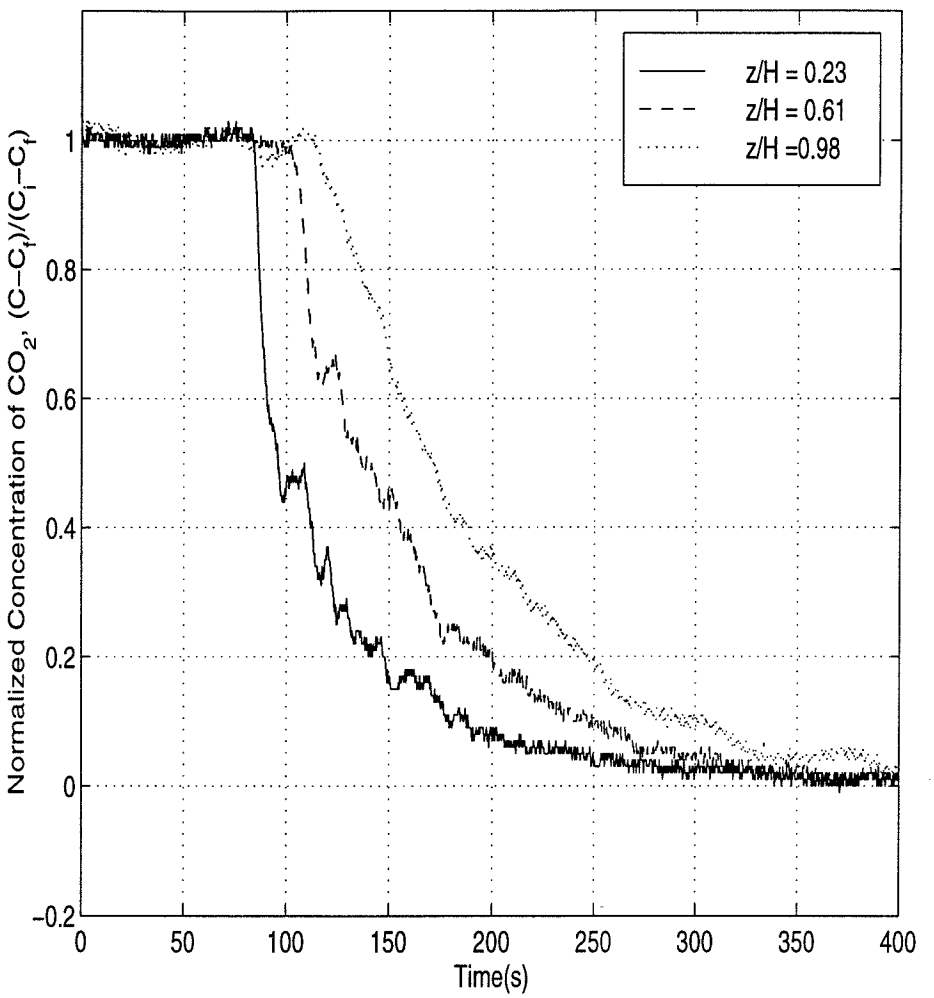

Figure 3.6: Tracer gas concentration as a function of time for the closed shaft with H/w = 10 and for the reservoir temperature = 80°C

The concentration of the tracer gas at a given location begins to fall as soon as the first hot front arrives at the location. For this experiment all the carbon dioxide is removed from the channel in about six minutes.

The quantity $(1 - \overline{C})$ can be compared to the temperature variation in the shaft. A normalized temperature is found by,

$$T^* = \frac{T - T_i}{T_f - T_i} \tag{3.6}$$

where T_f is the final temperature.

The quantities T^* and $(1 - C^*)$ are plotted versus time in fig. 3.7 for $\Delta\rho_i/\rho_{avg} = 0.312$. The time axis has been adjusted to account for the gas analyzer time delay of about 30 seconds.

The concentration exhibits a behavior similar to that of the temperature. The temperature rapidly reaches a steady state and slowly increases due to the increase in wall temperature. The concentration profile shows a slightly more gradual progression to the final state. These results seem to indicate that molecular diffusion is negligible and the turbulent mixing process dominates the flow.

3.2 Steady State

3.2.1 Temperature Distribution

After the first front reaches the top of the shaft a pseudo-steady- state is seen where the gas temperature fluctuates about a fairly constant value. Figure 3.8 shows the cross-section averaged temperature versus time, for the same experiment seen in fig. 3.1, for a longer time period. The steady state is observed at a given location shortly after the initial front reaches that location. However, during the steady state, the average temperature does increase slightly with time, corresponding to the rise of the wall temperature at that location. The fluctuations are $\pm$ 15-20 % of the mean temperature and have no preferred frequency. These fluctuations indicate that the

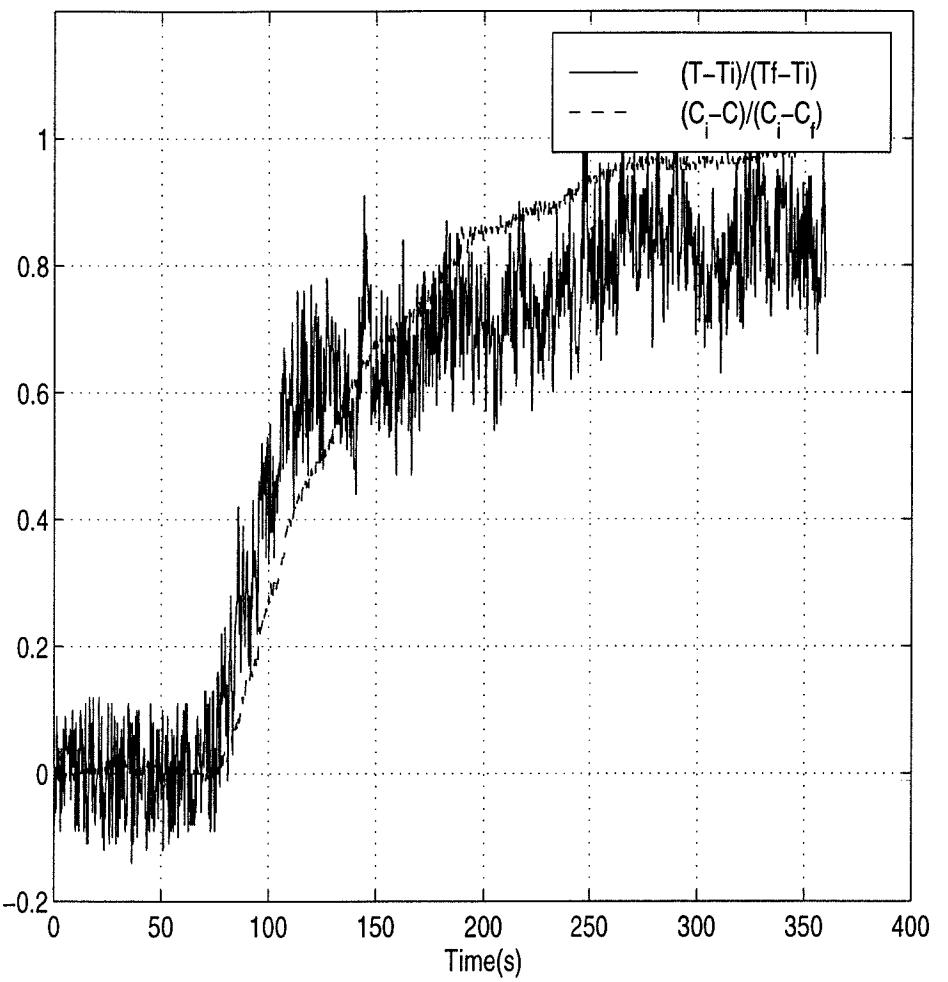

Figure 3.7: Comparison between temperature and concentration behavior as a function of time for the closed shaft at z/H = 0.98 and for the reservoir temperature = 120°C

turbulent mixing in the shaft continue for the duration of the experiments and the intensity of the mixing does not diminish with time. Limitations in the thermocouple response time (estimated as 0.2 s) did not allow higher frequency fluctuations (if any) to be observed.

The time average of this steady state temperature, T_{ss}, scales well with the initial temperature difference, $T_h - T_i$. Hence, the quantity, $(T_{ss} - T_i)/(T_h - T_i)$ for a given elevation z/H, is a constant independent of the temperature of the reservoir as shown in Fig. 3.9. The normalized steady state temperature decreases exponentially with height and is given by the equation:

$$\frac{(T_{ss} - Ti)}{T_h - T_i} = \exp\left[-a(z/H)\right] \tag{3.7}$$

Here, $a = 2.49$ for the 25.4 cm shaft and $a = 3.32$ for the 15.24 cm channel. Thus the steady state temperature decreases faster in the smaller channel.

The increase in wall temperature was small but not entirely negligible. The time averaged increase in wall temperature, $T_{w,ss} - T_i$ is about 3.5 % of $T_h - T_i$ at $z/H = 0.23$, and is lower for the higher elevations.

For a given cross section of the duct the time averaged temperature is highest near the center and lower closer to the wall (see fig. 3.10). The temperature distribution appears to be symmetric about the vertical axis through the center of the channel. The variation in temperature was no more than ± 8 % of the mean temperature for the cross - section.

3.2.2 Velocity Distribution

The velocity profile 104 cm ($z/H = 0.42$) from the bottom of the channel was obtained using constant temperature hot-wire anemometers. The anemometer records the velocity u where,

$$u = \sqrt{{u_y}^2 + {u_z}^2} \tag{3.8}$$

where u_y and u_z are the transverse and vertical components of velocity respectively.

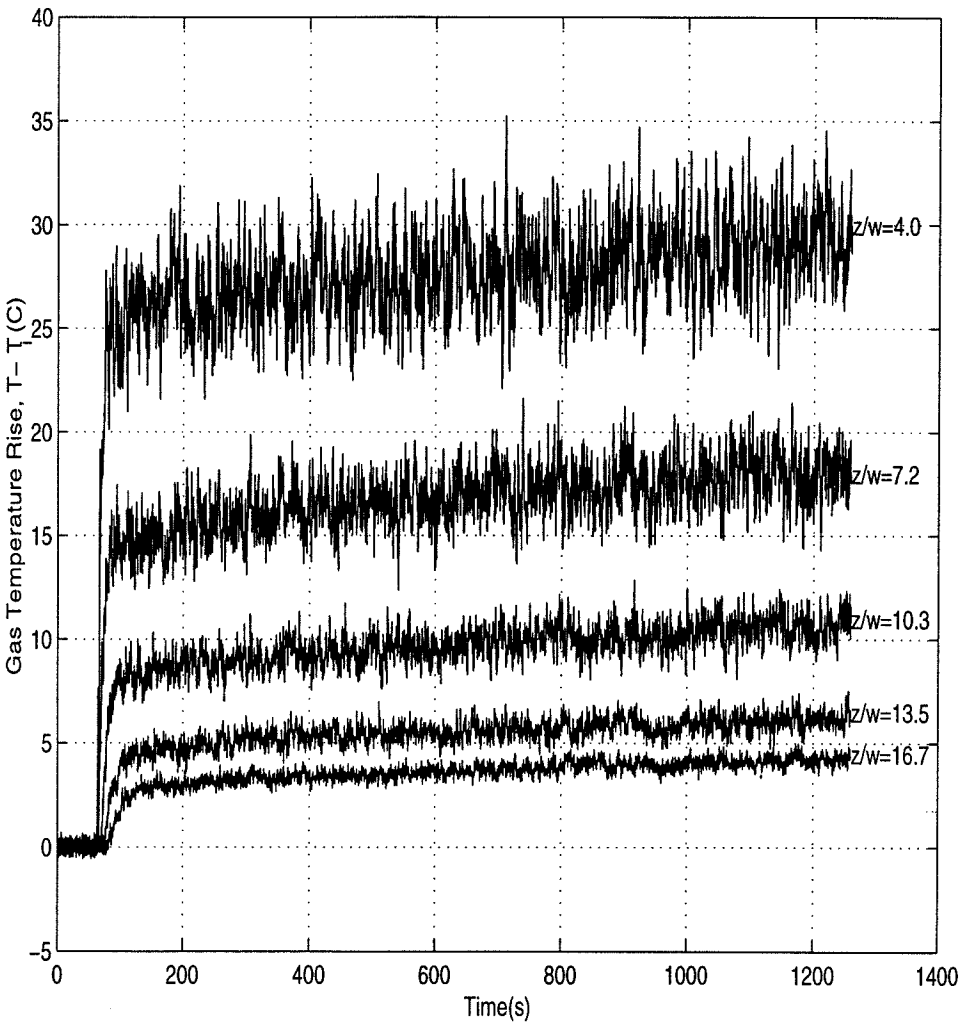

Figure 3.8: Steady state: average temperature as a function of time for the closed shaft with H/w =17 and for the reservoir temperature = 100°C

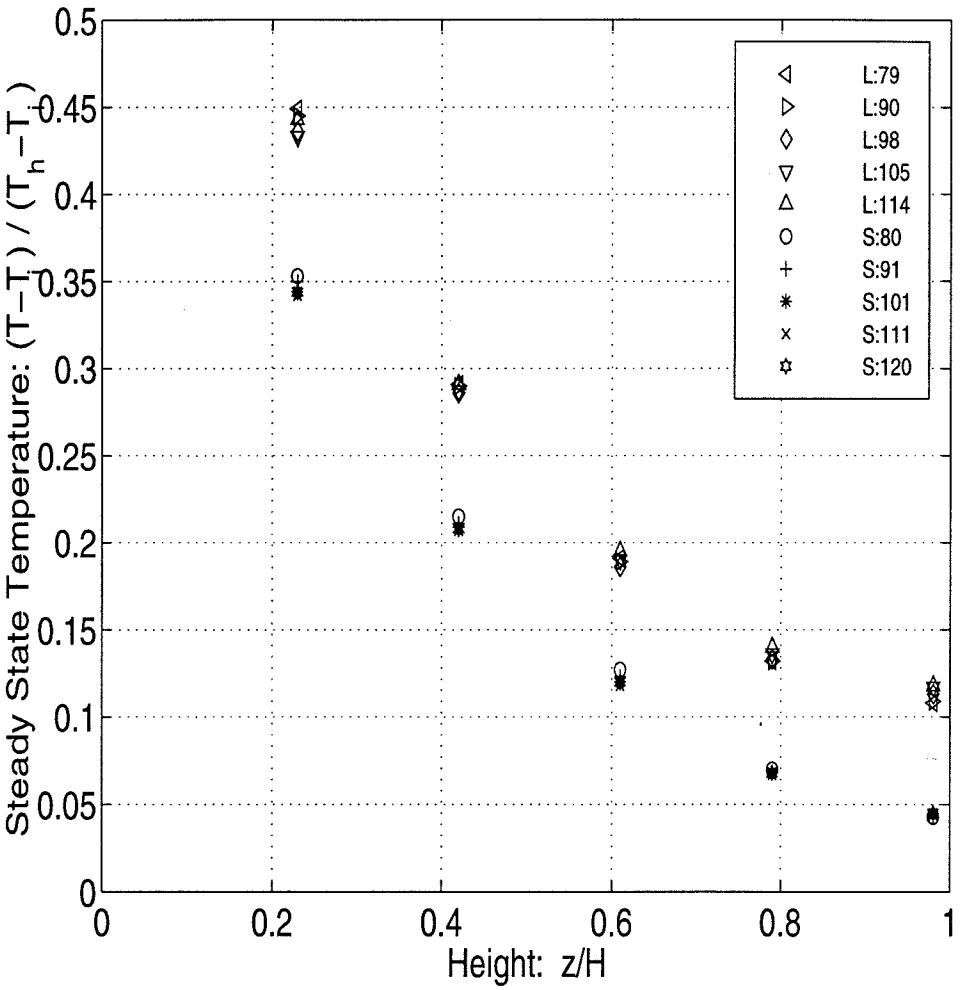

Figure 3.9: "Steady state" gas temperature for the closed shaft, for shaft sizes L = 25.4 cm and S = 15.24 cm and for various reservoir temperatures (^{o}C)

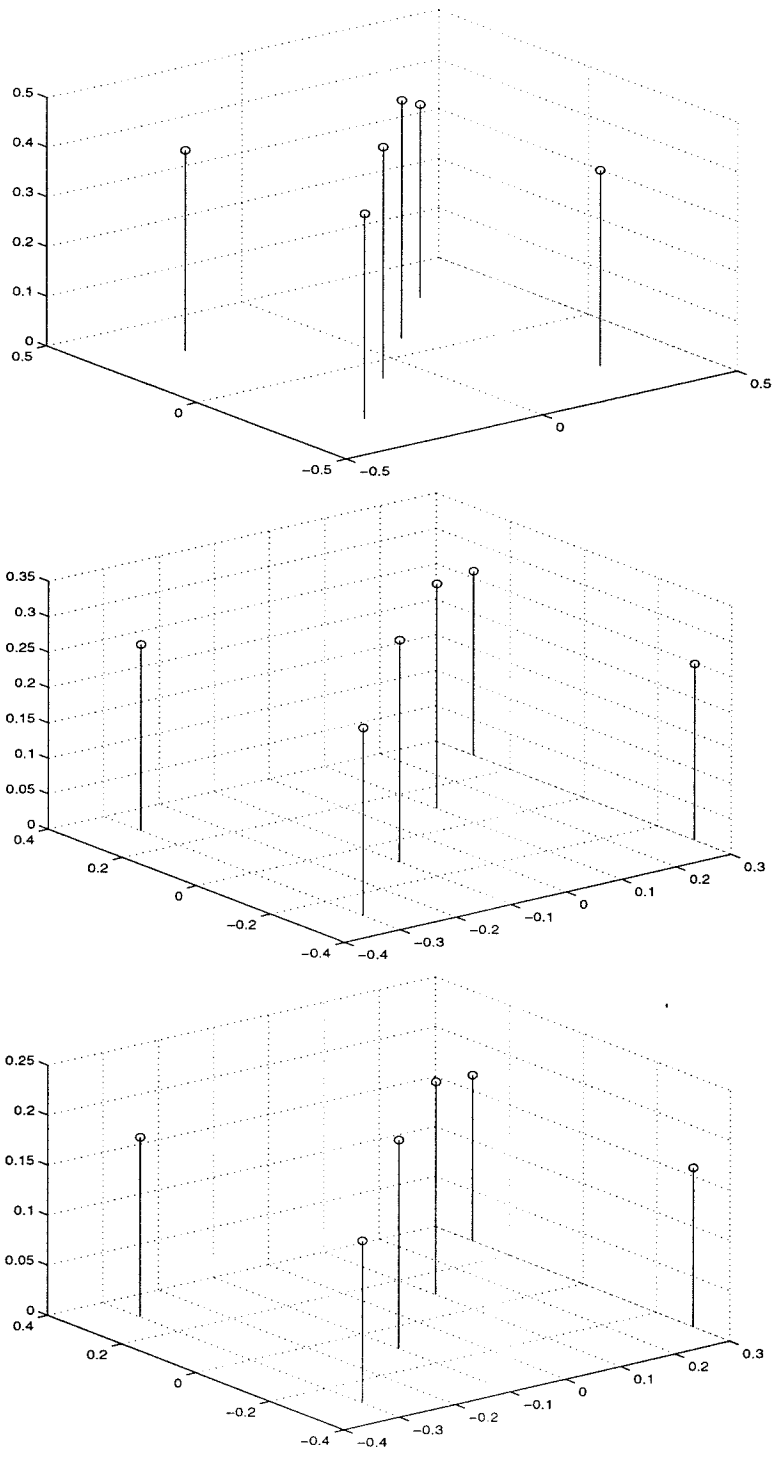

Figure 3.10: Cross sectional steady state temperature profile for 25.4cm shaft with reservoir temperature = 100°C, at (a) z/w = 2.4, (b) z/w = 4.3, (c) z/w = 6.2

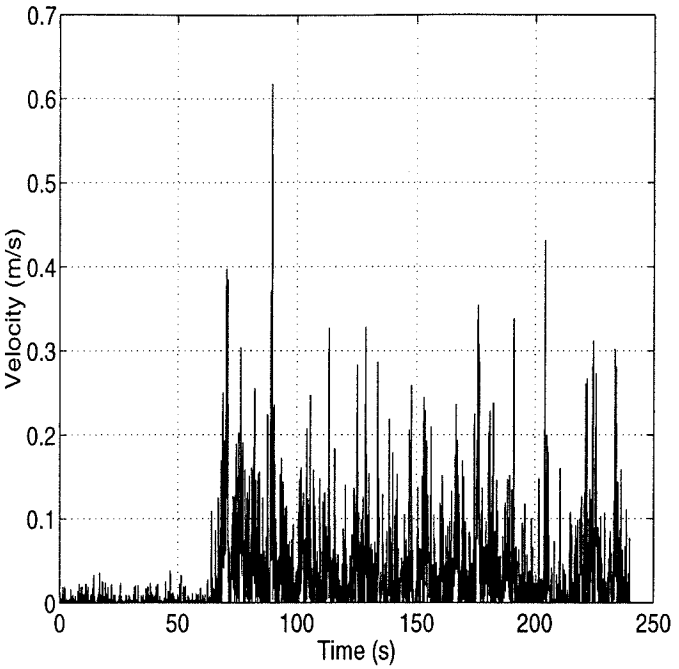

Figure 3.11: Velocity versus time for 25.4 cm channel at $z/H = 0.40$ and $r/w = 0.1$ with the reservoir temperature = 100°C

However, if u_z is much greater than u_y, then it can be assumed that $u \approx u_z$. Figure 3.11 shows a typical velocity versus time plot for a single anemometer placed at $r/w = 0.1$, where $r = w/2 - y$ is the distance from the wall. The figure shows that the velocity fluctuations increase in magnitude after the partition is removed at $t = 60$ s.

Measurements of the velocities are taken at various points in the cross section moving the probe in and out of the channel. Measurements are taken along a center-line of the shaft ($x/w = 0.5$) varying y/w and thus r/w. A mean velocity is obtained by averaging the instantaneous velocity over 60 s. The cross-sectional variation of mean velocity is displayed in fig. 3.12 (a) assuming a no slip condition at the wall. The velocity increases while progressing away from the wall possibly indicating the presence of a boundary layer. However, the velocity is maximum at $r/w = 0.3$ and decreases at the center of the channel ($r/w = 0.5$).

Since the hot-wire anemometer is not direction sensitive (i.e., it is unable to differentiate between upward and downward flow), the actual velocities are expected to

be lower than those seen in fig. 3.12(a). Moreover, the velocities in the closed shaft were significantly smaller than the lowest velocity obtained during calibration.

The quantity $u'_{rms}(y)/u_{ave}$ is plotted versus the non-dimensional distance from the wall in fig. 3.12(b). Here,

$$u'_{rms} = \sqrt{\frac{1}{n}[\sum_{i=1}^{n}(u_i - u_{ave})^2]} \tag{3.9}$$

is the root mean square value of the fluctuating velocity and u_{ave} is the average velocity at the cross-section. The measured fluctuations are all higher in magnitude than the average velocity, and the fluctuations are higher near the center, perhaps suggesting that the turbulent mixing is more intense away from the wall.

3.2.3 Heat Transfer

The local heat flux rate to the duct wall (q_w) was measured by the heat flow sensor at various heights in the channel. The heat transfer coefficient, h, is defined as

$$h = q_w/(T - T_w) \tag{3.10}$$

where T is the cross-section-averaged, gas temperature, and T_w is the local wall temperature.

The above equation assumes that convection is the dominant heat transfer mode and that radiation effects are negligible. Although this is a reasonable approximation for this study, where the highest temperatures observed were about 120 ^oC, it is not the case in real fires where temperatures can reach 1500 ^oC or higher.

The time averaged "steady state" Nusselt number is plotted in Fig. 3.13, where the Nusselt number based on the width of the duct is

$$Nu_w = hw/k \tag{3.11}$$

here k is the thermal conductivity of the gas at the film temperature T_f which is

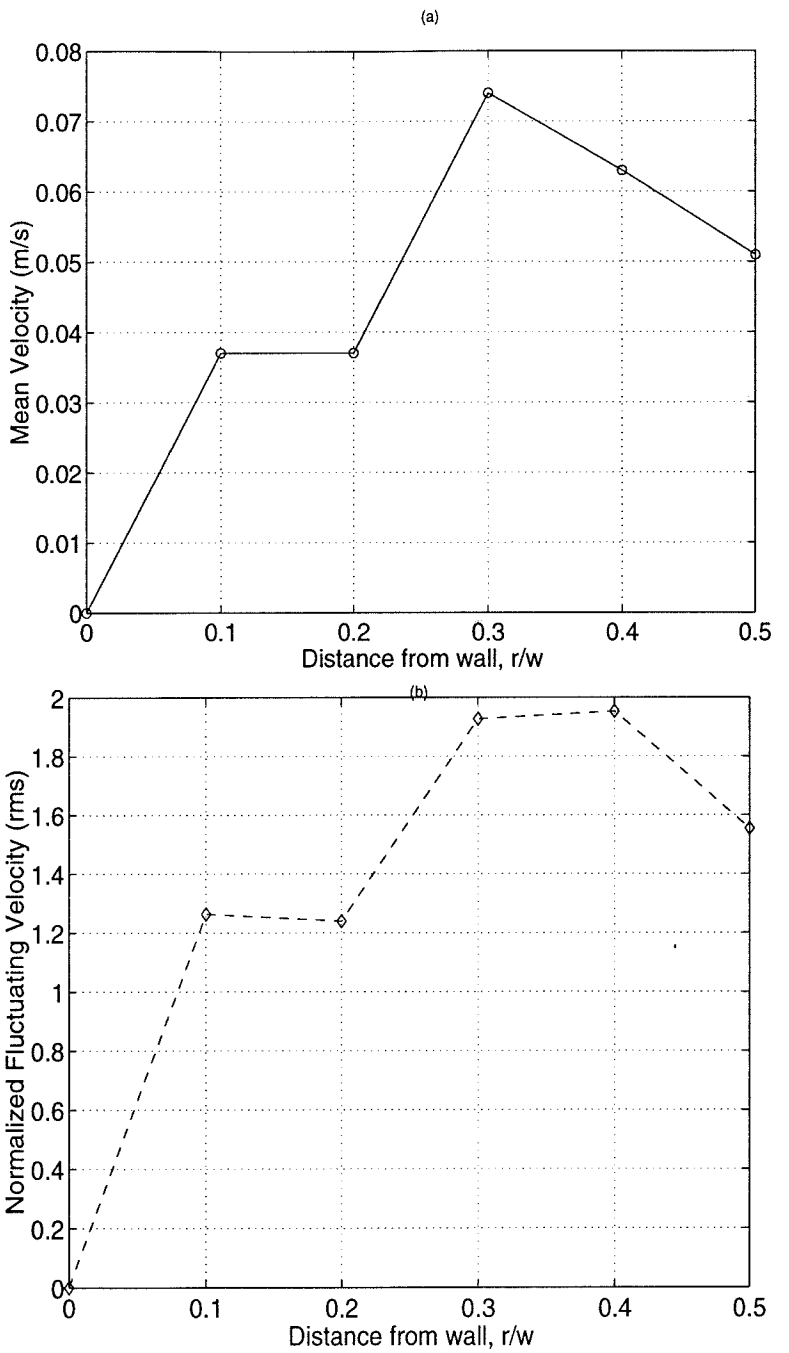

Figure 3.12: Cross sectional velocity profile for the 25.4 cm shaft at $z/H = 0.4$ with reservoir Temperature = 100^oC. (a) mean velocity (b) fluctuating velocity versus distance from the wall.

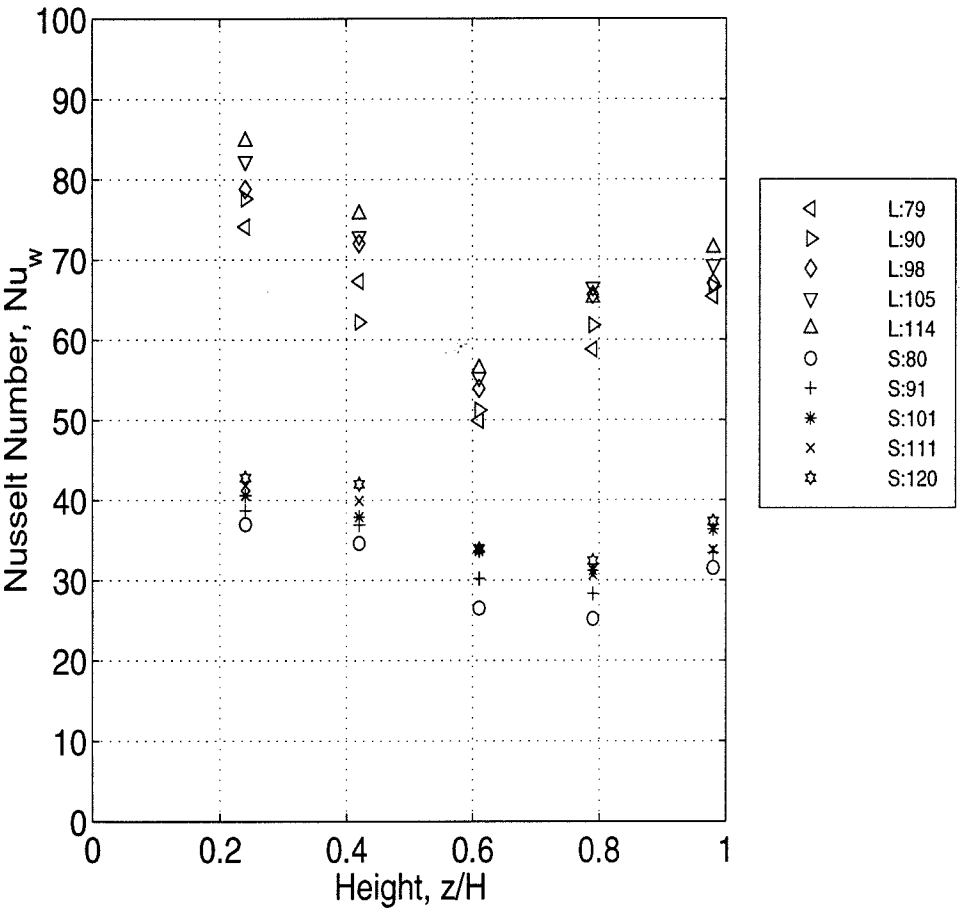

Figure 3.13: Steady state Nusselt number Nu_w versus location for shaft sizes L = 25.4 cm and S =15.4 cm and for various reservoir temperatures (^{o}C). Uncertainty for Nu is approximately $\pm$ 8 %

defined is the average of the gas and wall temperatures, i.e., $T_f = 0.5(T + T_w)$.

The figure shows that the values for the 15.24 cm shaft are approximately 60 % lower than those for the larger shaft. Hence, the heat transfer coefficient is almost independent of the size of the shaft. At a specified height the Nu_w increases slightly with increasing reservoir temperature.

For a single experiment the variation of the Nu_w with height is more complex. Progressing up the shaft it decreases, reaches a minimum a little past the mid-height, and increases again. The initial decrease may be due to the entrance effect and the subsequent increase is perhaps because of the presence of the top wall. These effects are more pronounced in the larger shaft, because it has a smaller aspect ratio. The heat flux, like the temperature, increased rapidly to a mean value shortly after the gate was opened, and fluctuated about this value for the rest of the experiment.

An important dimensionless quantity in free convection flows is the Grashof number defined as

$$Gr_w = \frac{g\beta(T_{ss} - T_{w,ss})w^3}{\nu^2} \tag{3.12}$$

here β is the volumetric thermal expansion coefficient and ν is the kinematic viscosity. The range 1.32x $10^6 < Gr_w <$ 7.07x 10^7 was investigated.

For natural convection in enclosures, the Nusselt number is a function of the Grashof and Prandtl numbers (Incropera and De Witt, 1990). The Prandtl number, $Pr = \nu/\alpha$, where α is the thermal diffusivity. The local Nusselt number is plotted versus the local Rayleigh number (Ra_z), where $Ra_z = Gr_z Pr$, in fig. 3.14.

The correlation given by the solid line in the figure is

$$Nu_z = 0.24(Ra_z)^{1/3} \tag{3.13}$$

In the above equation Nu_z is proportional to z and Ra_z is proportional to z^3. Hence, the length scale drops out of the equation indicating that the heat transfer coefficient, h, is independent of position.

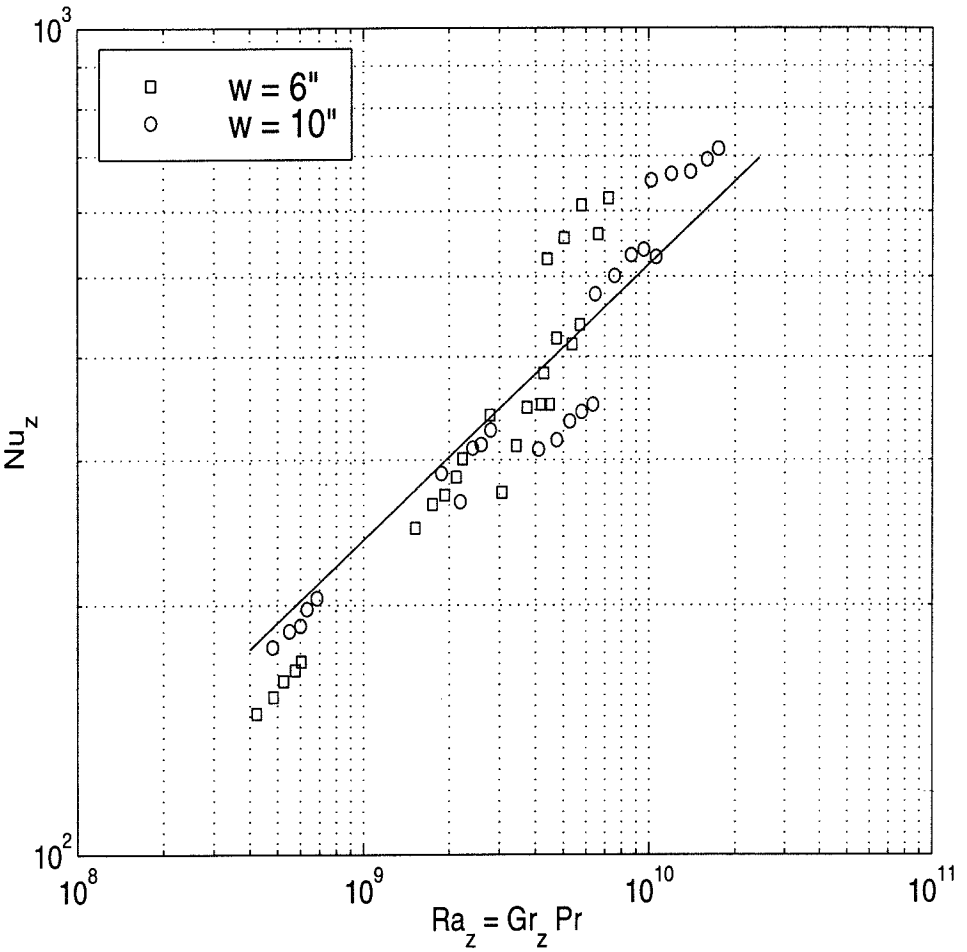

Figure 3.14: Local Nusselt number Nu_z as a function of local Ra_z for closed channel experiments

Chapter 4 Experimental Results: Vented Channel

The vented shaft experiments give insight into smoke propagation due the combined forces of stack effect and turbulent mixing. In the closed shaft experiments natural convection was the primary mode of heat transfer. However, in the case of the vented shaft, air is drawn out of the channel ensuing in forced convection as well. The venting of the shaft results in a non-standard mixed convection flow. In this experiment the forced convection is vertically upward. Furthermore, because the walls of the shaft are colder than the air inside, a downward thermal boundary layer is expected to exist near the wall. However, the flow is not a standard opposed convection flow because the mean flow has a negative temperature gradient with height. Nevertheless, the results of this study are compared with other mixed convection flow experiments.

An initial transient period was observed when the partition separating the vertical channel from the hot reservoir was removed and, as in the closed shaft experiments, a "steady state" situation prevailed subsequently.

4.1 Transient State

The mass flow-rate ($\dot{m}$) within the shaft is measured by the laminar flow element. The experimental results indicate that this $\dot{m}$ is constant with time to within 3%. Assuming there are no leaks in the shaft, this mass flow rate is the same at any cross-section of the channel from the conservation of mass. The local mean velocity is then given by $\overline{u} = \dot{m}/(\rho w^2)$, where ρ is the local density, which is a function of temperature. The local Reynolds number can then be found by

$$Re_w = \frac{\overline{u}w}{\nu} \tag{4.1}$$

where ν is the kinematic viscosity of the gas. For a given experiment, the local Reynolds number along the shaft did not vary more than 3% from the average value ($Re_{w,avg}$).

The location of the initial front non-dimensionalized by the width of the duct is plotted versus the time from when the partition was opened, in fig. 4.1 for various values of $Re_{w,avg}$. The data for $Re = 0$ corresponds to the closed shaft. For the fastest withdrawal rate ($Re = 7223$), the front reaches the top more than eight times faster than that for the closed shaft, while the arrival time for the $Re = 1000$ flow is halved from the closed shaft value. Since the temperature of the hot reservoir T_h was approximately the same for all the experiments shown, it is evident that the stack effect has a significant impact on the propagation rate of the initial front.

The time for the first front to reach the top of the shaft is plotted versus the average Reynolds number in fig. 4.2 for the smaller shaft. The time taken for the closed shaft ($Re = 0$) is shown for comparison.

If the experiment were conducted with an unheated reservoir, the reservoir gases would have no buoyancy. Since the flow is incompressible, the velocity of the flow inside the shaft would be independent of position. Given the Reynolds number Re, the mean velocity would be obtained by $\overline{u} = (Re)(w)/\nu$. The time for the shaft to be evacuated of its contents would then be $t_{evac} = H/\overline{u}$ where H is the height of the channel. This evacuation time is shown by the dotted line in the fig. 4.2. Although this evacuation time and the front arrival time is almost the same for the highest flow-rate, the evacuation time is considerably greater for the smaller flow-rates. Hence, the buoyancy and the turbulent mixing is significant in the propagation of the front for vented shafts as well.

Effect of Window Position

The position of the opening where the venting takes place has an impact on the progression of the initial front. The arrival times for three sets of experiments for the larger (25.4cm) channel are indicated in fig. 4.3. The first set is for the vented shaft with the opening near the top, at $z/H = 0.95$. The second set is for the shaft vented

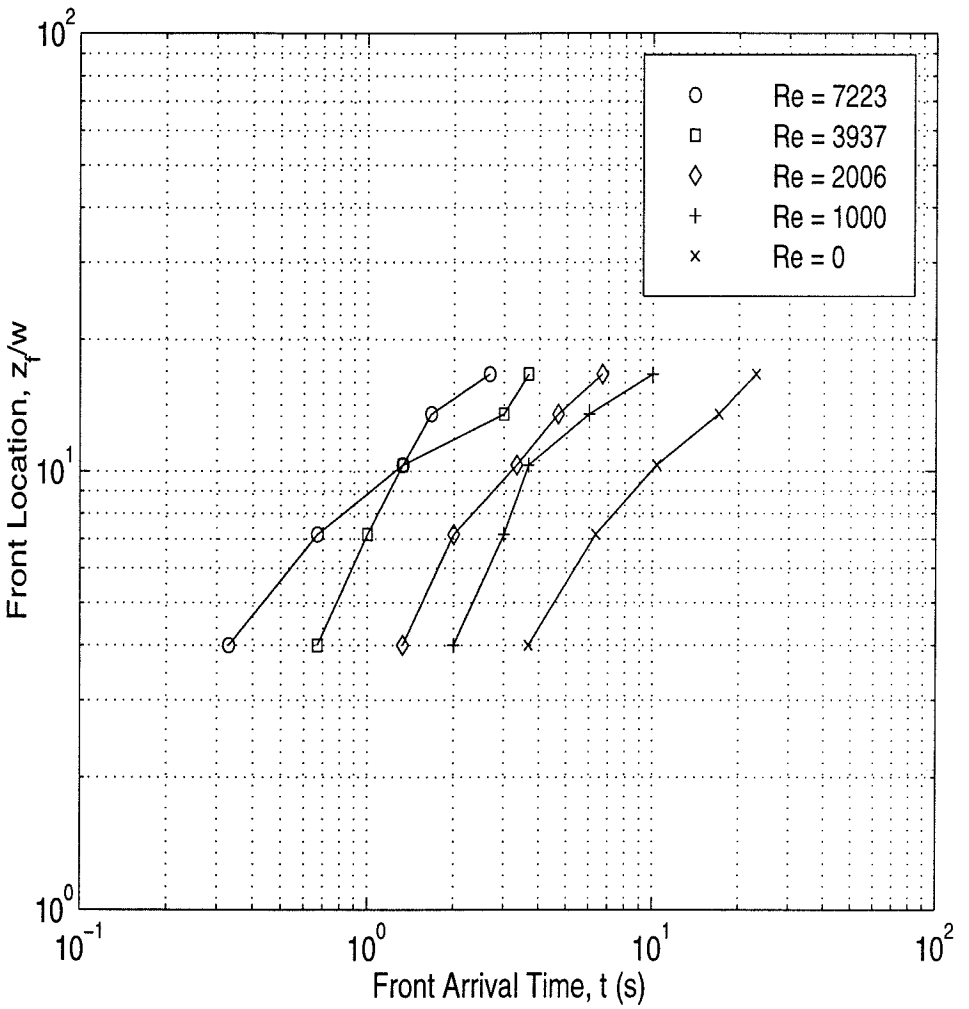

Figure 4.1: Progress of the initial front versus time for vented shafts at various Re, where Re is the average Reynolds number based on the width of the duct. H/w =17 and $T_h \approx 100^o$ C

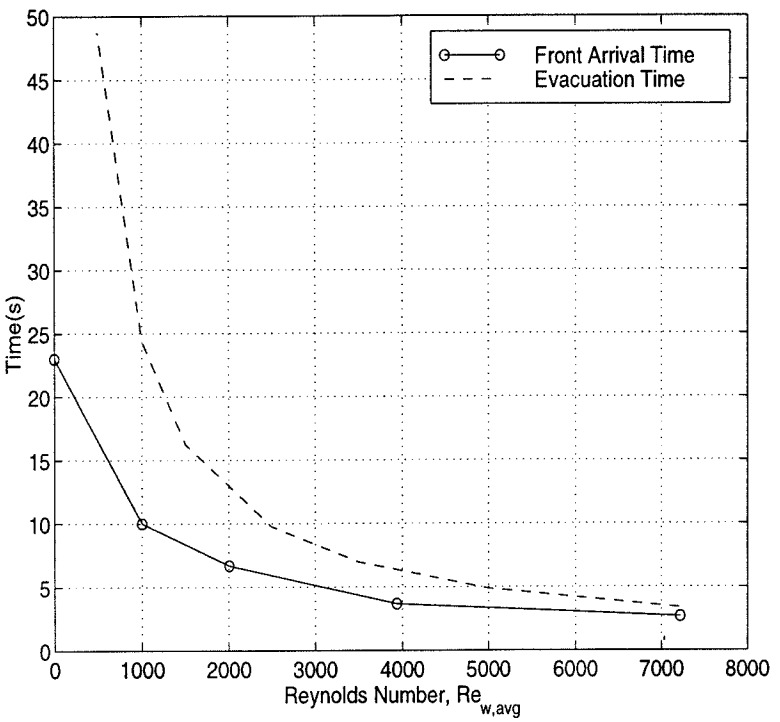

Figure 4.2: Arrival time of front at the top, $z/H = 0.98$ versus average Reynolds number for the vented shaft. The time for the shaft to be evacuated of its contents is also shown. H/w =17 and $T_h \approx 100^o$ C

at two-thirds of the height, $z/H = 0.67$, and the final set is for the closed shaft.

A comparison of data for similar Reynolds numbers indicates that the initial front progresses at approximately the same rate up to $z/w = 6.2$. However, the front for the top vented shaft arrives at the upper elevations in a shorter time. The initial fronts for the top vented shaft reach the top of the shaft in about half the time that the fronts for the shafts vented at $z/H = 0.67$. The arrival time for the closed shafts are greater than any of the vented shafts. Thereby the venting always decreases the arrival time but has a more pronounced effect if the opening is at an upper elevation.

4.2 Steady State

4.2.1 Temperature Distribution

The temperature profile at z/H = 0.23 is plotted versus time for both vented and closed shafts in fig. 4.4. The temperature for the vented shaft experiments also rise to a "steady state" in a short time with the transient period being even smaller than that of the closed shaft. As the flow withdrawal rate, and hence the Reynolds number, is increased, the average temperature at a cross section increases from the closed shaft values. This increase is probably due to the forced convection introduced by the venting process. The venting appears to have a "damping" effect on the temperature since the fluctuating component of temperature decreases as the Reynolds number is increased.

The "steady state" behavior of the vented shaft experiments can be compared by taking a time average of mean temperature rise at a cross section and normalizing it with $T_h - T_i$. This normalized temperature rise for the smaller shaft is plotted versus vertical location for various values of Re in fig. 4.5. The venting causes a dramatic rise in the temperature even for a the slowest flow-rate shown corresponding to $Re = 1000$.

Although the quantity, $(T_{ss}-Ti)/(T_h-T_i)$, increases with Re, attempts to scale the non-dimensional temperature with Reynolds number were unsuccessful. The thermal

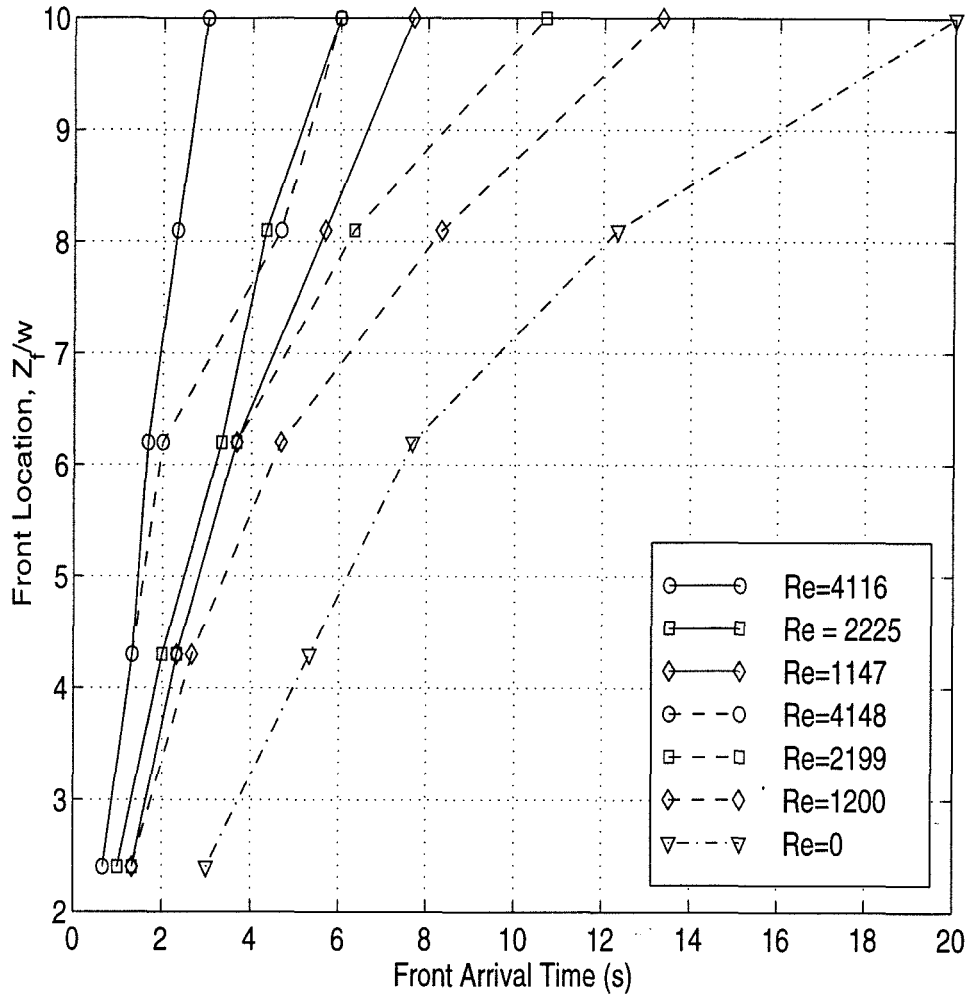

Figure 4.3: Progress of the initial front versus time for vented shafts at various Re. H/w = 10.2 and $T_h \approx 100°$ C. The solid line corresponds to the shaft vented at z/H=0.95, the dashed line to the shaft vented at z/H=0.67 and the dash-dot line to the closed shaft.

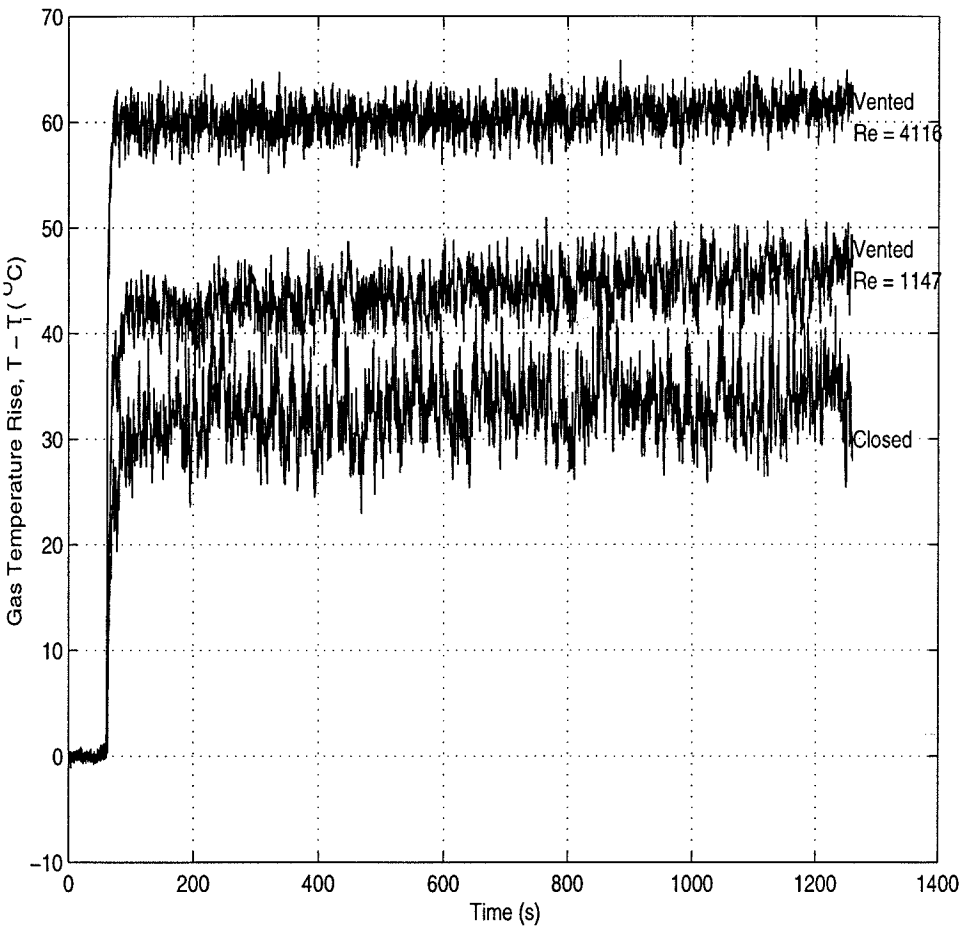

Figure 4.4: Average temperature rise versus time at z/H =0.23 for vented (opening at z/H =0.95) and closed channels with H/w=10.2 and $T_h \approx 100^o$.

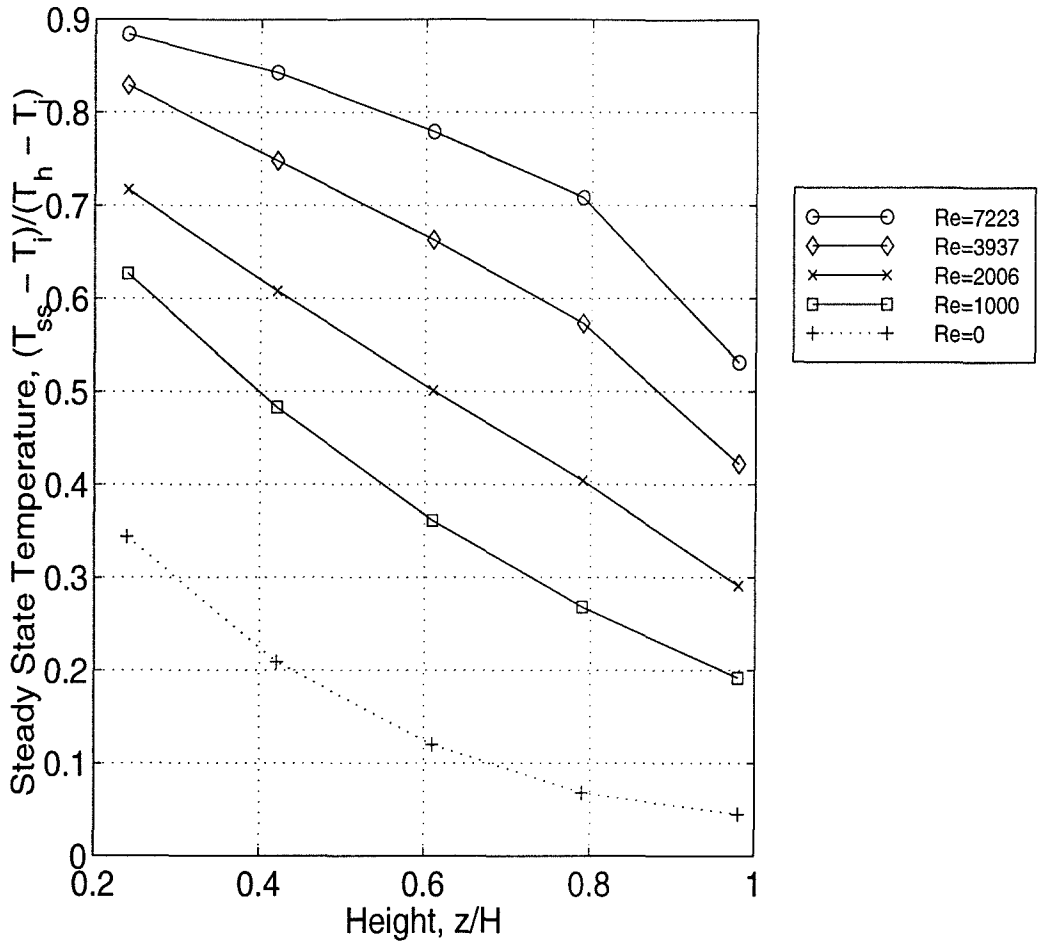

Figure 4.5: Time-averaged steady state temperature for vertical channel (H/w= 17) vented at $z/H = 0.95$, for various values of the average Reynolds number

energy removed from the reservoir varies for different flow-rates, which could be a reason why the temperatures did not scale.

4.2.2 Velocity Distribution

A typical velocity-time plot for the vented shaft is displayed in fig. 4.6. This plot is obtained by a hot wire probe placed at $z/H = 0.42$ and $r/w = 0.1$. The velocity is qualitatively similar to the corresponding closed shaft plot. However, the mean velocity is larger in this case.

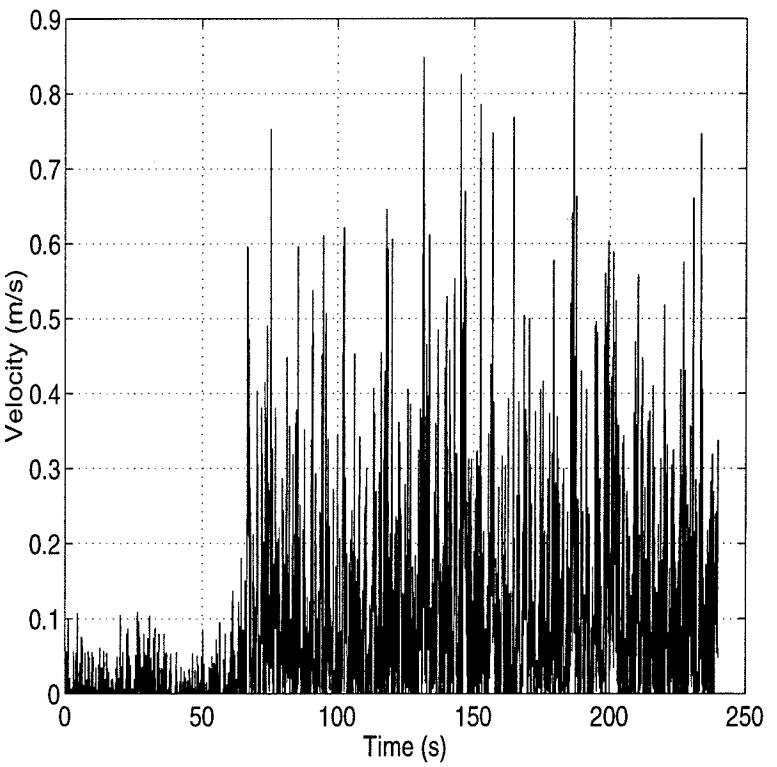

Figure 4.6: Velocity versus time for 25.4 cm channel at $z/H = 0.42$ and $r/w = 0.1$ for $Re = 2225$ and $T_h = 100^o$C

The velocity profile at a cross section at $z/H = 0.42$ is shown in fig. 4.7. The local mean velocity, $\overline{u}(y)$, is plotted as a function of the distance from the wall in fig. 4.7(a). Not surprisingly, the velocity is higher at the greater Reynolds number. The velocity profile is almost flat for the unheated flow, whereas for the cases with a hot reservoir the velocity is higher near the center. It is apparent that the temperature gradients do affect the velocity profile, possibly due to the presence of a thermal boundary layer.

Figure 4.7(b) shows the rms value of the fluctuating velocity, u'_{rms}, normalized by the mean velocity at the cross section, $\overline{u}$. The figure shows the fluctuations are greater near the center of the channel and are increased by the presence of temperature gradients. Furthermore, higher withdrawal rates appear to reduce the relative magnitude of the fluctuations.

4.2.3 Heat Transfer

In mixed convection flows the quantity, Gr_w/Re_w^2, is an indication of the relative importance of the free and forced convection in the flow. If $Gr_w/Re_w^2 >> 1$, forced convection effects can be neglected, and vice versa (Incropera and DeWitt, 1990). In this study, the range, $0.26 < Gr_w/Re_w^2 < 151$, was investigated, with Re_w varying from 590 to 7250 and Gr_w from 6.63x10^6 to 7.61x10^7. Therefore, a correlation of the form, $Nu_w = Nu_w(Re_w, Gr_w, Pr)$, was expected.

The time averaged Nusselt number for the smaller shaft is plotted as a function of vertical location for various values of the Reynolds number in fig. 4.8. In the smaller shaft, the Nusselt number varies between 35 and 40 for all of the flow rates except for the values at z/H =0.98. These correspond to a location about 5 cm from the top of the channel where the heat transfer is enhanced due to proximity of the wall. This "ceiling effect" is greater for the higher Reynolds numbers. The results for the other parts of the duct show no dependence on the Reynolds number. The experimental values of Nusselt numbers for the larger shaft were in the 55-70 range except for those near the top which were higher. A comparison of the two shaft sizes indicates that

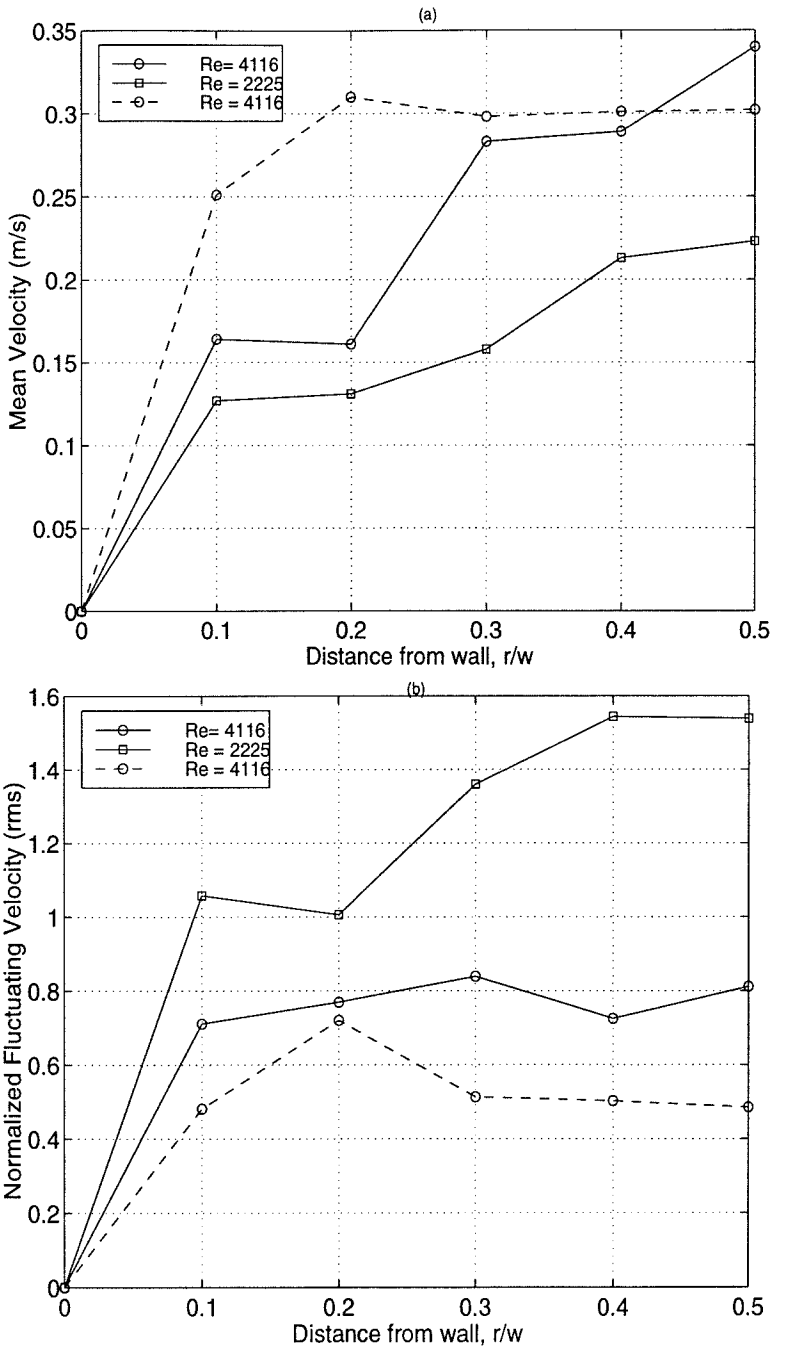

Figure 4.7: Velocity profile at a cross section for 25.4 cm channel at $z/H = 0.42$ for two flow rates. $T_h = 100^oC$. The dashed line corresponds to an unheated flow. (a) Mean velocity, $\overline{u}(y)$ and (b) Normalized velocity fluctuation, $u'_{rms}/\overline{u}$

the Nusselt numbers for the smaller channel are about 60 % of the values for the larger channel as is the case for the closed shafts.

The experimental values of the Nusselt number based on the vertical coordinate are plotted versus the Rayleigh number in fig. 4.9 for both shaft sizes. The data shown are only for the top vented shafts and the values for $z/H = 0.98$ were not included since these gauges were above the vent and the nature of the flow above the vent was different from that below the vent.

The correlation,

$$Nu_z = 0.18 Ra_z^{1/3} \tag{4.2}$$

is also shown in the figure and fits the data well.

This is same as the correlation obtained for the closed shaft heat transfer except that the constant of proportionality is 75% lower.

Similar results have been obtained by other researchers studying mixed convection heat transfer. Brown and Gauvin (1965) conducted experiments in both aided and opposed convection in a heated vertical duct with a circular cross-section for $380 < Re < 6900$. The channel was open at the top and bottom and the walls were maintained at a constant temperature. They reported a good correlation of their data with

$$Nu = c_{bg} Ra^{1/3} \tag{4.3}$$

for $Ra > 10^6$. Here the constant c_{bg} was 0.13 for aided convection and 0.19 for opposed convection.

As a comparison the the Nusselt number for turbulent pipe flow with pure forced convection with a mean fluid temperature greater than the wall temperature is

$$Nu_d = 0.023 Re_d^{0.8} Pr^{0.3} \tag{4.4}$$

where d is the diameter of the pipe.

Although the venting and hence the stack effect had a significant impact on the front arrival time and the steady state temperature in the channel, the heat transfer

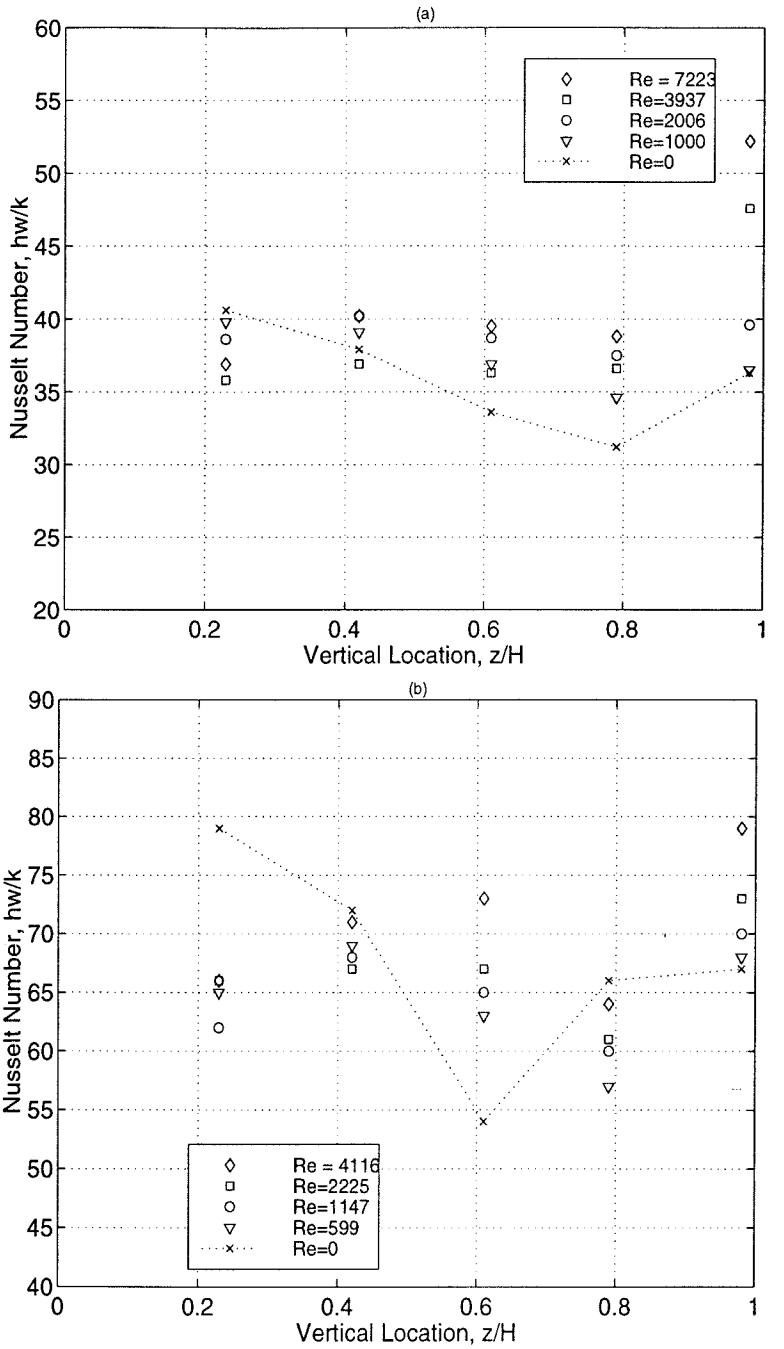

Figure 4.8: Time-averaged Nusselt number versus vertical location for the vented channels at various Reynolds numbers for $T_h = 100\ ^oC$. (a) 15.24 cm channel (b) 25.4 cm channel. $Re = 0$ corresponds to the closed shaft data

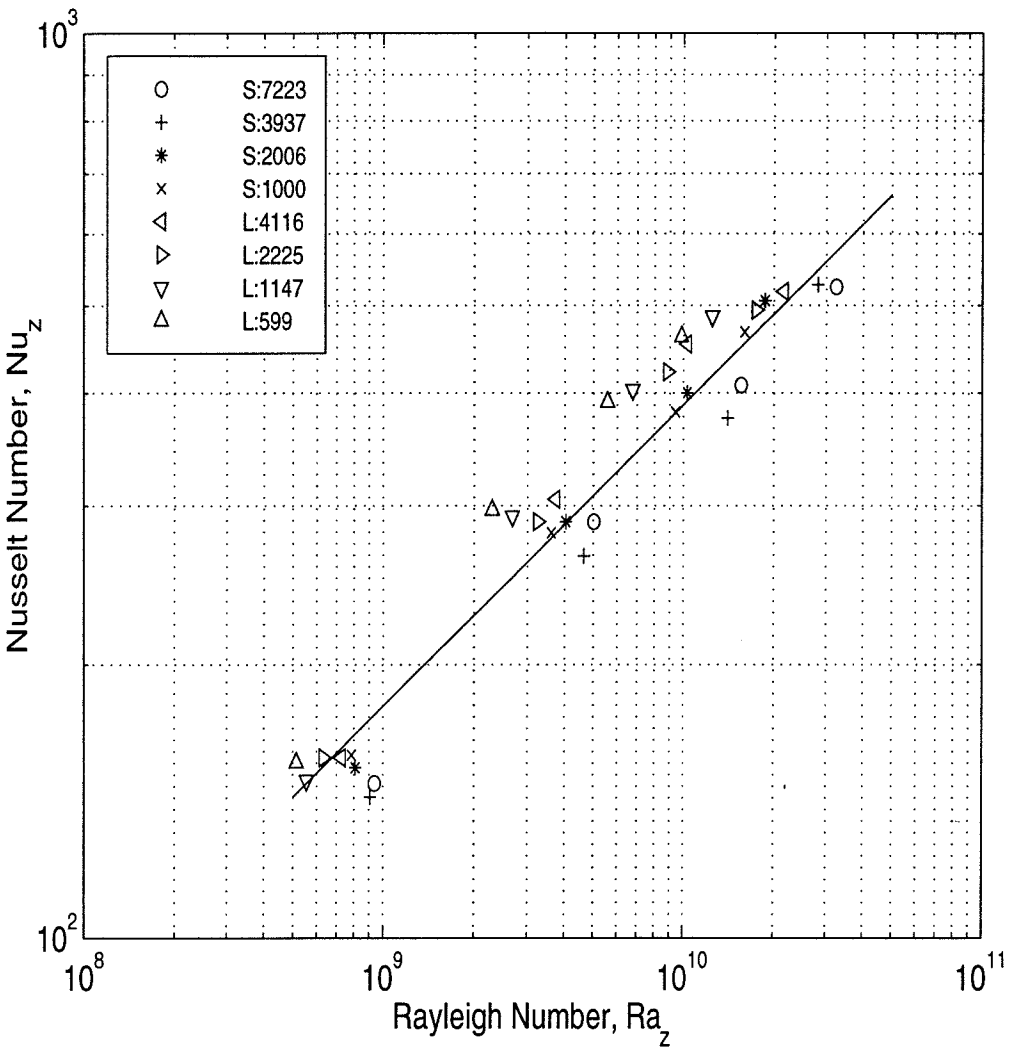

Figure 4.9: Time-averaged local Nusselt number versus local Rayleigh number for the vented channels: S = 15.24cm and L = 25.4cm at various values of Re_w

coefficient was independent of the flow-rate. Natural convection appeared to be the dominant heat transfer mode for the vented flows even for Reynolds number as high as 7250.

Chapter 5 Analytical Model

A theoretical analysis of buoyant shaft flows was performed to complement the experimental work. The closed and vented shafts were treated separately, although both cases were modeled using simple conservation of energy arguments. The analysis was limited to the steady state where the fluid temperature is assumed to be invariant with time.

5.1 Closed Shaft

The closed shafts were used to study smoke propagation by turbulent mixing alone. A theoretical analysis of the turbulent mixing was performed based on an instability model, similar to that used by Cannon (1975). Since the flow is turbulent, properties such as velocity and temperature are defined as a sum of mean and fluctuating components. For example,

$$\begin{aligned} u &= \overline{u} + u' \\ T &= \overline{T} + T' \end{aligned} \tag{5.1}$$

5.1.1 Assumptions

The following simplifying assumptions were made:

1. The flow is one-dimensional in the vertical direction.

2. The mean velocity in the vertical direction is zero.

3. Turbulent diffusion dominates the flow and hence molecular diffusion is negligible.

4. The wall temperature is constant with position and equal to the initial ambient temperature.

From experimental results, the temperature gradient in the vertical direction was dominant and hence the flow was assumed one-dimensional for simplicity. The second assumption is justified because there is no net mass flux through any cross section of the shaft. Therefore, $\overline{u} = 0$ and $u = u'$. The third simplification is one often encountered in turbulent flows and can be inferred from the experiments with tracer gas. And finally the temperature change at the wall was very small for the duration of the experiment and hence can be assumed to be negligible.

5.1.2 Formulation

Consider an energy balance on an elemental height, Δz, of the shaft as shown in fig. 5.1. With the above assumptions the turbulent transport of heat in the vertical direction is balanced by the heat transfer to the wall. An energy balance can be written as

$$\rho c_p w^2 \Delta z \frac{\partial}{\partial z}(\overline{u'T'}) = -4w\Delta z q_w \tag{5.2}$$

which simplifies to

$$\rho c_p \frac{\partial}{\partial z}(\overline{u'T'}) = -\frac{4q_w}{w} \tag{5.3}$$

Here ρ and c_p are the mean density and the specific heat at constant pressure respectively.

The heat transfer to the wall, $q_w = h(\overline{T} - T_w)$, where h is the heat transfer coefficient, $\overline{T}$ is the mean component of the gas temperature and T_w is the wall temperature.

The $\overline{u'T'}$ term can be defined in terms of an eddy thermal diffusivity, ϵ_H,

$$\overline{u'T'} = -\epsilon_H \frac{\partial}{\partial z}(\overline{T}) \tag{5.4}$$

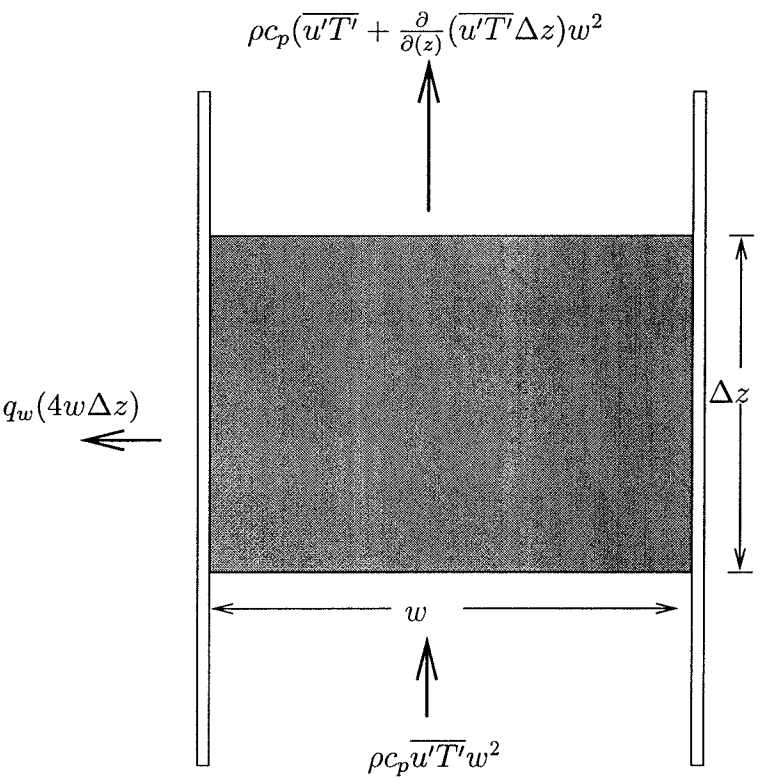

Figure 5.1: Energy Balance

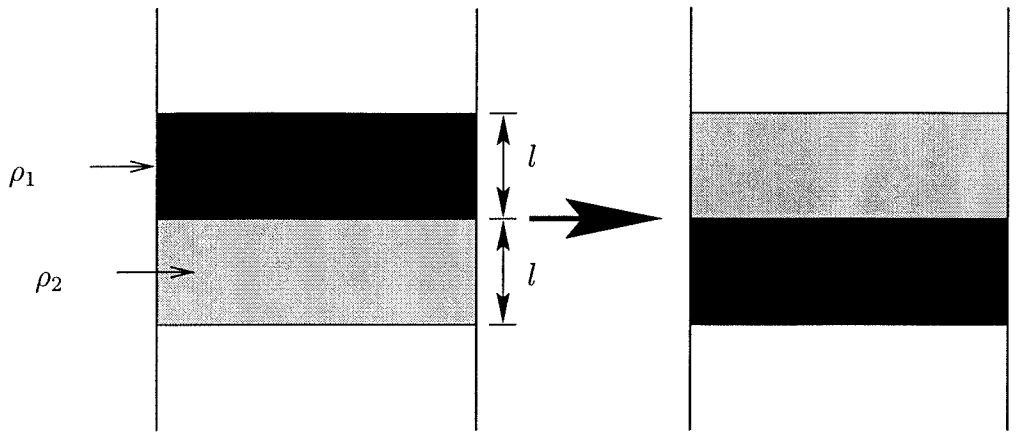

Figure 5.2: Determination of u'

Substituting in equation (5.2), the equation becomes

$$\rho c_p \frac{\partial}{\partial z}(\epsilon_H \frac{\partial \overline{T}}{\partial z}) = \frac{4h}{w}(\overline{T} - T_w) \tag{5.5}$$

The eddy thermal diffusivity follows the corresponding eddy momentum diffusivity and is assumed to be proportional to the product of the characteristic velocity fluctuation, u', and a mixing length, λ.

The value for u' is determined by examining an unstably stratified section of fluid as shown in fig. 5.2 and is based on the potential energy change when a mass of fluid with a vertical scale, l, and density, ρ_1, moves downward in the shaft and displaces a fluid with the same scale but a smaller density, ρ_2.

The velocity fluctuation, u', is found by equating the potential energy change to the kinetic energy of the fluctuations. i.e.,

$$\rho u'^2 \propto (\rho_1 - \rho_2) g l \tag{5.6}$$

Since $(\rho_1 - \rho_2) \propto (\partial \rho / \partial z) l$,

$$u' \propto \sqrt{\frac{1}{\rho}\frac{\partial \rho}{\partial z} g l^2} \tag{5.7}$$

The diffusivity becomes, $\epsilon_H \propto \sqrt{((g/\rho)\partial\rho/\partial z)}l\lambda$, or from the ideal gas equation of state,

$$\epsilon_H = c_1\sqrt{(\frac{-g}{\overline{T}}\frac{\partial \overline{T}}{\partial z})}l\lambda \tag{5.8}$$

where c_1 is a constant. Substituting for ϵ_H in equation (5.5)

$$\rho c_p \frac{\partial}{\partial z}(c_1\sqrt{(\frac{-g}{\overline{T}}\frac{\partial \overline{T}}{\partial z})}l\lambda\frac{\partial \overline{T}}{\partial z}) = \frac{4h}{w}(\overline{T} - T_w) \tag{5.9}$$

The temperature and height are normalized by $\tau = \overline{T}/T_i - 1$ and $\zeta = z/H$. Assuming $T_w \approx T_i$ the equation becomes

$$c_1\rho c_p l\lambda (g)^{1/2}(1/H)^{5/2}\frac{\partial}{\partial \zeta}[\sqrt{\frac{-1}{(\tau+1)}\frac{\partial \tau}{\partial \zeta}}\frac{\partial \tau}{\partial \zeta}] = \frac{4h\tau}{w} \tag{5.10}$$

A relationship is now required for the heat transfer coefficient, h. Since a known analytical model does not exist for this type of flow, dimensional analysis was utilized to obtain a correlation by assuming a form,

$$h \propto \rho c_p u_1 (u'/u_1)^{\gamma} \tag{5.11}$$

where $u_1 = (g/H)^{1/2}l$ and γ is a constant.

From equation (5.7), $u' \propto \sqrt{(-g/\overline{T})(\partial \overline{T}/\partial z)l^2}$, or, non-dimensionally, $u'/u_1 \propto \sqrt{(-1/(\tau+1))(\partial\tau/\partial\zeta)}$.

The results from the closed shaft experiments are displayed as $h/(\rho c_p (gH)^{1/2})$ versus $\sqrt{(-1/(\tau+1))(\partial\tau/\partial\zeta)}$ in fig. 5.3. The correlation

$$h/(\rho c_p (gH)^{1/2}) \propto (\sqrt{(-1/(\tau+1))(\partial\tau/\partial\zeta)})^{0.5} \tag{5.12}$$

shown by the solid line in the figure agrees with the data. Thus, $\gamma = 0.5$ and

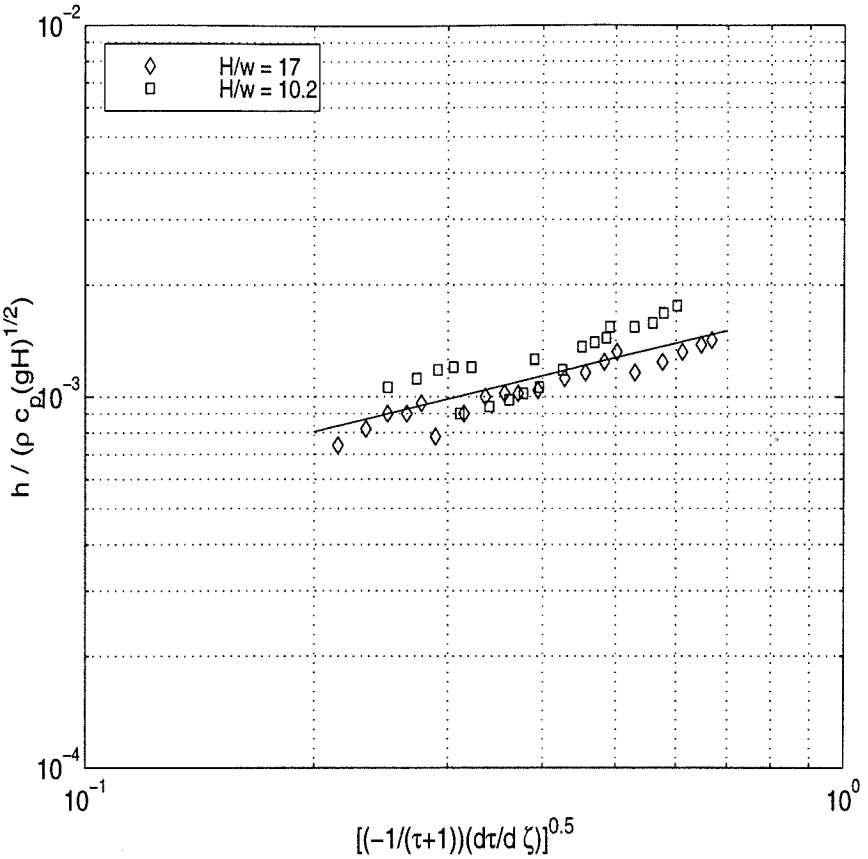

Figure 5.3: Dependence of the heat transfer coefficient on the velocity fluctuation for closed shafts

$$h = c_2 \rho c_p \left(\frac{g}{H}\right)^{1/2} l \left(\frac{-1}{(\tau+1)} \frac{\partial \tau}{\partial \zeta}\right)^{1/4} \tag{5.13}$$

where c_2 is a constant.

Substituting for h in equation (5.10) and simplifying,

$$\frac{\partial}{\partial \zeta}\left[\sqrt{\frac{-1}{(\tau+1)} \frac{\partial \tau}{\partial \zeta}} \frac{\partial \tau}{\partial \zeta}\right] = \frac{4 c_2 H^2}{c_1 \lambda w}\left[\frac{-1}{(\tau+1)} \frac{\partial \tau}{\partial \zeta}\right]^{1/4} \tau \tag{5.14}$$

Taking derivatives and simplifying further,

$$\frac{\partial^2 \tau}{\partial \zeta^2} - \frac{1}{3(\tau+1)} \left(\frac{\partial \tau}{\partial \zeta}\right)^2 = c\tau \left[\frac{-1}{\tau+1} \frac{\partial \tau}{\partial \zeta}\right]^{-1/4} \tag{5.15}$$

Here $c = (8c_2H^2)/(3c_1\lambda w)$, and $0 < \zeta < 1$. The boundary conditions are

1. $T(z = 0) = T_h$, or $\tau(0) = T_h/T_i - 1$ with T_h being the reservoir temperature.

2. $T(z = H) = T_w = T_i$, or $\tau(1) = 0$

The terms on the left-hand side of the second-order non-linear differential equation (5.15) correspond to the turbulent transport of heat and the term on the right-hand side is related to the heat transfer to the wall. The -1/4th power on the wall heat transfer term is a consequence of the form assumed for the heat transfer coefficient. This equation was solved using an equation solver in MATLAB. Since the constant c is not known, the boundary condition $\tau'(0)$ was obtained by a curve fit of the experimental results. Then the value of c that satisfied the boundary condition $\tau(1) = 0$ was obtained using a shooting technique.

5.1.3 Results

Fig. 5.4 shows the analytical results for various values of the constant c for the 25.4 cm shaft with a reservoir temperature of 100°C and $c = 4.47$ satisfied the boundary condition at $\tau = 1$. Comparing all the closed shaft experiments,

$$c = \begin{cases} 4.37 \pm 0.14 & \text{For w = 25.4 cm} \\ 8.90 \pm 0.53 & \text{For w = 15.24 cm} \end{cases}$$

The value of c is larger for the smaller shaft because $c \propto 1/(\lambda w)$ and λ, the mixing length, is expected to increase with shaft width. Fig. 5.5 shows that the normalized temperature is slightly lower for the smaller duct; a trend also seen in the experimental results. Moreover, since $c = (8c_2H^2)/(3c_1\lambda w)$, and $c_2H/l = 0.00182$ from (5.13) and fig. 5.3, $(c_1 l\lambda)_{w=25.4cm} = 0.076$ and $(c_1 l\lambda)_{w=15.24cm} = 0.062$. Therefore the eddy diffusivity is defined as a function of the temperature gradient.

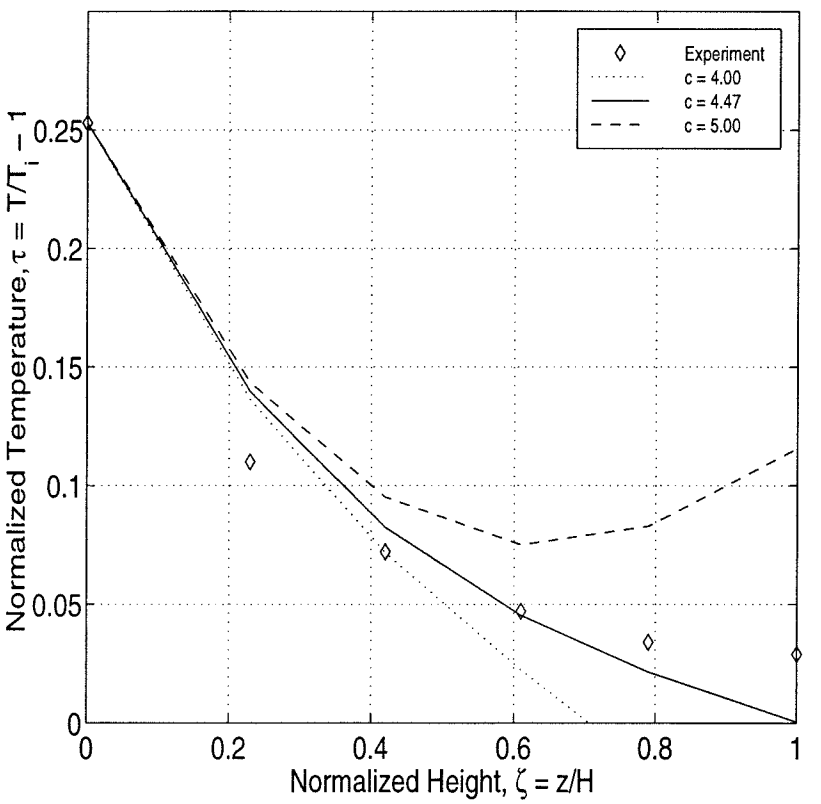

Figure 5.4: Predicted steady state temperature for the closed shaft, H/w = 10.2 and $T_h \approx 100°C$, for different values of C. The corresponding experimental results are also shown

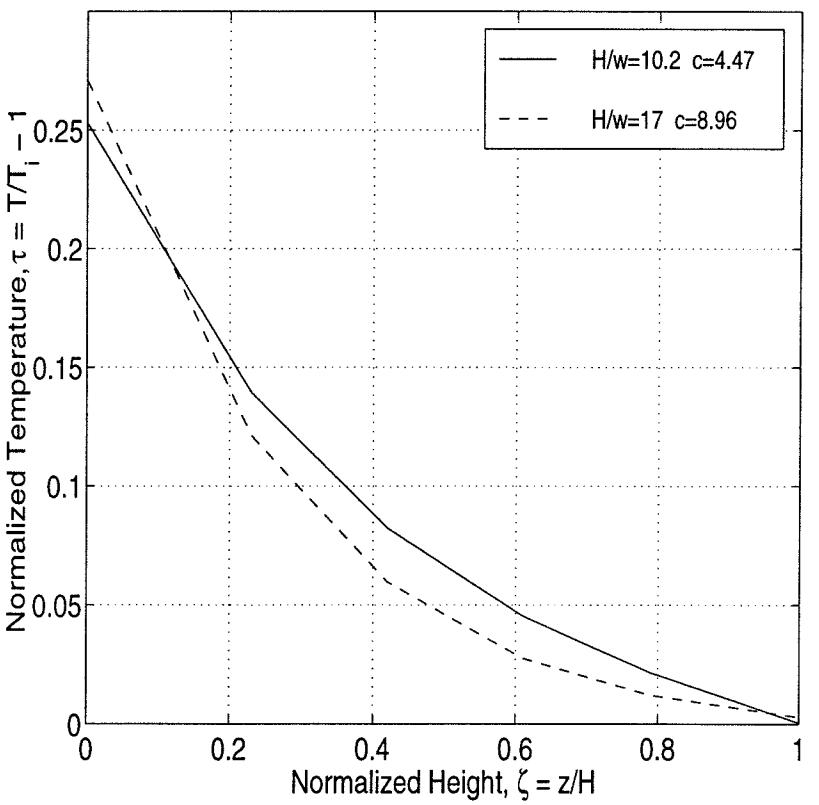

Figure 5.5: Predicted temperature variation for the closed shafts for the two shaft sizes

5.2 Vented Shaft

The vented shafts were used to study smoke propagation due to the combined effects of the stack effect and turbulent mixing. The assumptions used are the same as those for the closed shaft, except that the mean vertical velocity is no longer zero. This mean velocity, however, is assumed to be invariant in the vertical direction throughout the channel.

5.2.1 Formulation

An energy balance is once again performed on an elemental section of the duct, and in the case of vented flow the convective term in the energy equation is non zero. The simplified energy balance yields.

$$\rho c_p \overline{u} \frac{\partial \overline{T}}{\partial z} + \rho c_p \frac{\partial}{\partial z}(\overline{u'T'}) = -\frac{4q_w}{w} \tag{5.16}$$

Here, $q_w = h(T - T_w)$ and the Reynolds temperature term can be written in terms of an eddy thermal diffusivity, ϵ_H. This eddy diffusivity is given by equation (5.8). Substituting for q_w and ϵ_H in equation (5.16),

$$\rho c_p \frac{\partial}{\partial z}(c_1 \sqrt{(\frac{-g}{\overline{T}} \frac{\partial \overline{T}}{\partial z})} l\lambda \frac{\partial \overline{T}}{\partial z}) - \rho c_p \overline{u} \frac{\partial \overline{T}}{\partial z} = \frac{4h}{w}(\overline{T} - T_w) \tag{5.17}$$

Non-dimensionalizing,

$$c_1 \rho c_p l\lambda (g)^{1/2} (1/H)^{5/2} \frac{\partial}{\partial \zeta}[\sqrt{\frac{-1}{(\tau+1)} \frac{\partial \tau}{\partial \zeta}} \frac{\partial \tau}{\partial \zeta}] - \frac{\rho c_p \overline{u}}{H} \frac{\partial \tau}{\partial \zeta} = \frac{4h\tau}{w} \tag{5.18}$$

Once again a suitable correlation was sought for the heat transfer coefficient, h. Since both free and forced convection is involved, h is expected to depend on both the mean and fluctuating velocities, i.e., $h = h(\overline{u}, u')$. The experimental results, however, indicated no dependence of h on the Reynolds number for values of Re_w up to 7000. Therefore, h is assumed to be independent of u.

Fig. 5.6 shows the normalized heat transfer coefficient $h/(\rho c_p (gH)^{1/2})$ plotted

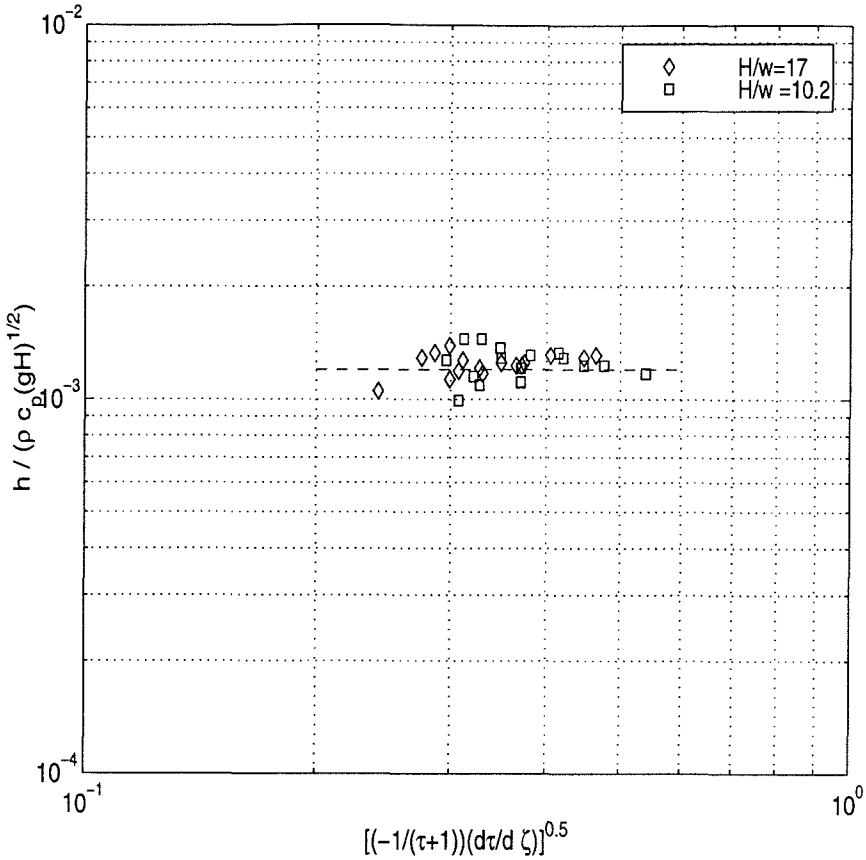

Figure 5.6: Dependence of the heat transfer coefficient on the velocity fluctuation for vented shafts

versus $\sqrt{(-1/(\tau+1))(\partial\tau/\partial\zeta)}$ for the open shaft experiments. The trend seen for the closed shaft results is not seen here and the heat transfer coefficient is independent of the fluctuating velocity.

Also the experimental values for $h/(\rho c_p(gH)^{1/2})$ fall within 20% of 0.0061. For convenience it is assumed that $h/(\rho c_p)$ is constant. Simplifying equation (5.18),

$$\frac{\partial^2\tau}{\partial\zeta^2} - \frac{1}{3(\tau+1)}\left(\frac{\partial\tau}{\partial\zeta}\right)^2 - c_v\frac{\partial\tau}{\partial\zeta}\left[\frac{-1}{\tau+1}\frac{\partial\tau}{\partial\zeta}\right]^{-1/2} = c_q\tau\left[\frac{-1}{\tau+1}\frac{\partial\tau}{\partial\zeta}\right]^{-1/2} \tag{5.19}$$

Here $c_v = (2\overline{u}H)/(3C_1l\lambda\sqrt{g/H})$ and $c_q = (8H^2)/(3c_1l\lambda w\sqrt{g/H}) * (h/(\rho c_p))$. For a given velocity c_v and c_q are completely specified.

The first two terms of the differential equation (5.19) are identical to those of the

PDE describing the closed shaft. The third term is the convective component and is a function of the mean velocity of the flow. The term on the right-hand side is a function of the wall heat transfer.

5.2.2 Boundary Conditions

The flow in the vented shafts is relatively more complex, and the end boundary conditions are dependent on the flow velocity. The flow at the entrance must satisfy,

$$\rho c_p u \frac{\partial T}{\partial z} = k_H \frac{\partial^2 T}{\partial z^2} + Q_{wall} \tag{5.20}$$

where k_H is an eddy conductivity.

Integrating from $z = 0^-$ to $z = 0^+$,

$$\frac{1}{T - T_h} \frac{\partial T}{\partial z} = \frac{\rho c_p u}{k_H} = \frac{u}{\epsilon_H} \tag{5.21}$$

Substituting for ϵ_H from (5.8) and normalizing T and z,

$$\left(\frac{1}{\tau - \tau_h} \frac{\partial \tau}{\partial \zeta} \sqrt{\frac{-1}{(\tau+1)} \frac{\partial \tau}{\partial \zeta}}\right)_{z=0^+} = \frac{H\overline{u}}{c_1 l \lambda \sqrt{(g/H)}} \tag{5.22}$$

Flow out of the vent cannot be modeled with one-dimensional flow. Therefore, $\partial T/\partial z \rightarrow 0$ as $z \rightarrow$ inf, was selected as the second boundary condition.

A value is assumed for τ at the entrance such that $\tau(0^+) < \tau_h$, thereby specifying $\partial\tau/\partial\zeta(0^+)$ from (5.22). The solution for the differential equation was attempted by iterating for the entrance condition such that the condition at infinity is satisfied. However, this endeavor was unsuccessful because real (non-complex) solutions to the equations existed only for a small window of $\tau(0)$. Therefore, the infinity boundary condition was ignored, and the above mentioned iteration was conducted to obtain the best fit for the experimental results.

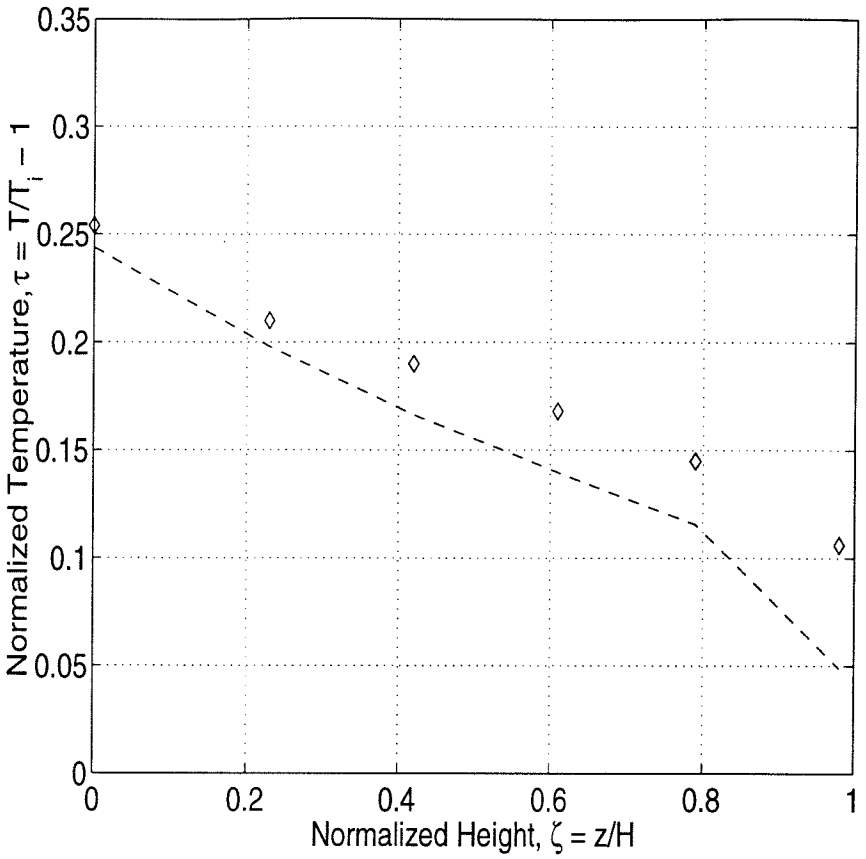

Figure 5.7: Analytical results for 15.24 cm channel vented at $z/H = 0.95$ with $Re = 3937$. Experimental results are also shown for reference

5.2.3 Results

The analytical results for the 15.24 cm shaft with $Re = 3937$ is displayed in fig. 5.7. The model predicts a lower temperature than obtained by experiment. The analytical results for all the top vented shafts are depicted in fig. 5.8. Higher Reynolds numbers resulted in higher temperatures. The temperature profiles are qualitatively similar to experimental results, with the higher flow-rates yielding linear profiles and the lower flow-rates producing exponential profiles. However, the model underestimated the local temperature in all cases. The entrance condition, forces $\tau(0^+)$ to become very much lower than τ_h for the lower flow-rates. The assumption of one-dimensional flow breaks down in the region of the vent, and could cause the disagreement between

analytical and experimental results. Furthermore, the instability model utilized to determine u' did not take the the flow-rate into account.

Although reasonable qualitative agreement was obtained by the model with experiment, the theory and experiment did not compare well quantitatively, particularly in the case of vented shafts.

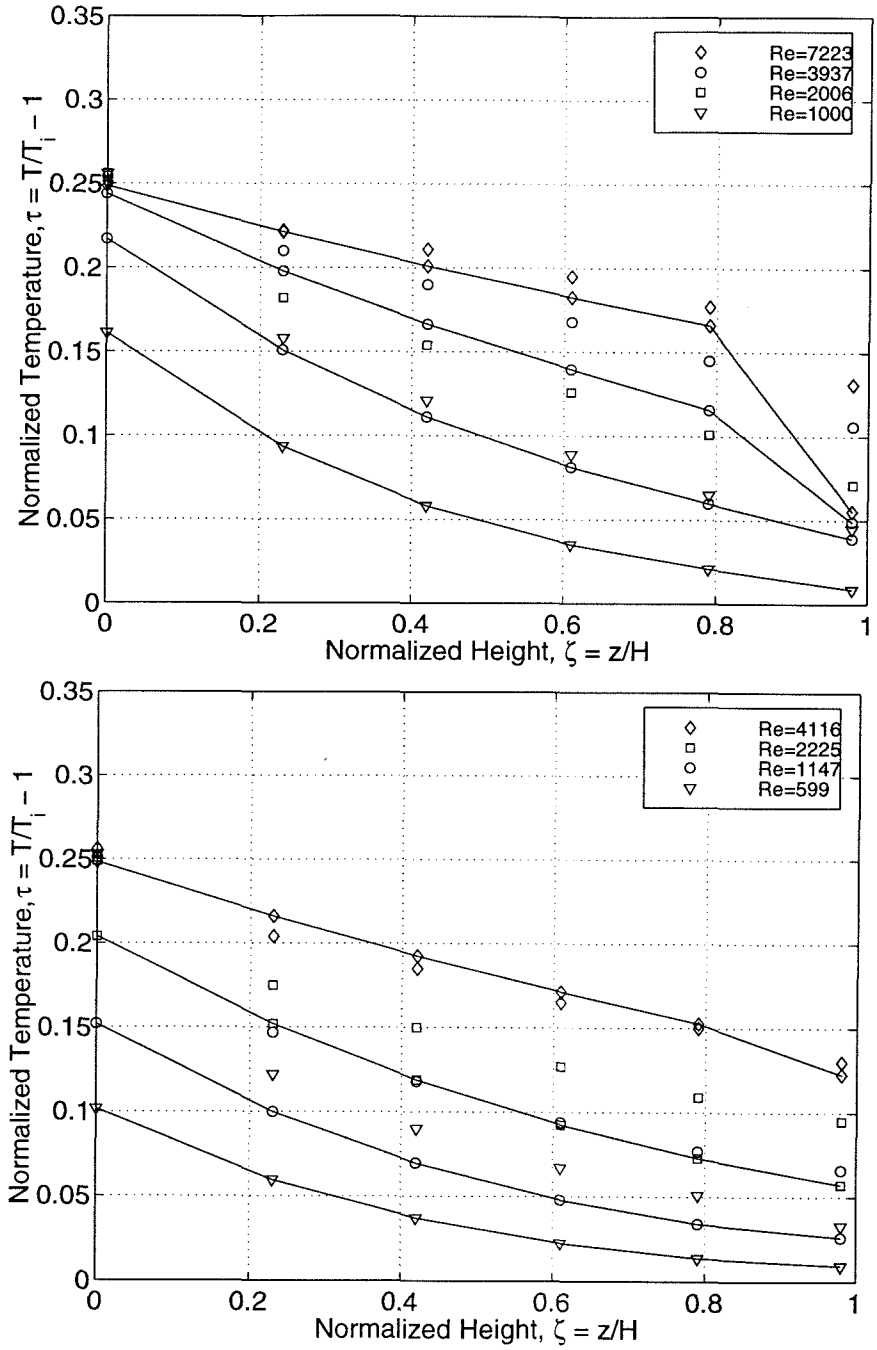

Figure 5.8: Analytical results for channels vented at $z/H = 0.95$ for various Re. (a) 15.24 cm shaft (b) 25.4cm shaft. The corresponding experimental data is shown with the same legend sans the solid line.

Chapter 6 Summary and Conclusions

This investigation was primarily concerned with smoke movement in vertical channels during fires in high rise buildings. The work included both experimental and theoretical aspects with an emphasis on the former. The study was motivated by the widespread damage to life and property caused by accidental building fires. The stack effect and turbulent mixing, two of the factors primarily responsible for the propagation of smoke within tall buildings, were examined.

Many additional safety features are incorporated into designing high-rise buildings, and this investigation attempts to provide useful information in the design of building fire codes. This work is an extension of some mass transfer experiments on the same topic by Cannon and Zukoski utilizing mixtures of water and salt-water.

The experimental facility consisted of a tall vertical channel with aspect ratios of 10.2 and 17, and a large reservoir initially separated by a partition. The vertical channel contained ambient air while the reservoir was filled with heated air. In a few cases a trace quantity of carbon dioxide was added to the channel. The experiment began when the partition was removed and the hot air from the reservoir rose into the shaft. The progression of the hot gas fronts and mixing of the hot and cold air were monitored by arrays of thermocouples located at several cross sections within the shaft. Heat flow sensors measured the heat flux at the wall, and some velocity measurements were made with hot wire anemometers. A carbon dioxide analyzer was used in the tracer gas tests. A data acquisition system recorded the temperature, velocity and heat flux.

In most real fires the turbulent mixing and stack effect occur together. However, in order to examine each effect separately, two types of experiments were conducted. The first consisted of closed vertical shafts. These channels were sealed, limiting the possibility of leaks and thereby eliminating the stack effect. In the second set of tests, the vertical channels were vented at different locations and air was withdrawn at

controlled rates from these openings. These experiments examined the combination of the stack effect and turbulent mixing.

In both the closed and vented channels, a brief transient period was observed initially followed by a pseudo steady state. The temperature and the heat flux first increased and then fluctuated about their steady state values.

For the closed channels, a correlation was obtained for the front propagation rate. The location of the initial front was a function of the initial temperature ratio, the channel width and a gravitational constant. Comparison of the hot gas front propagation with Cannon's experiments indicated that the heat transfer to the wall reduced the progress rate of the initial front. The steady state temperature scaled well with the reservoir temperature. The Nusselt number was approximately constant as a function of elevation with small variations due to entrance and ceiling effects. The velocities observed in the channel were small and in the order of 0.05 m/s. The velocity fluctuations were of the same order of magnitude as the mean velocities.

In vented shaft flows the withdrawal of the gas had a significant impact on the front progression rate and on the steady state temperatures. The venting also appeared to have a damping effect on both the velocity and temperature fluctuations. However, an increase in the flow rates by a factor of eight did not produce a significant change in the heat transfer coefficient, which was also independent of the elevation. The heat transfer results correspond well with previous work and suggest that the free convection effects dominated the flow even for Reynolds numbers up to 7000.

A one-dimensional analytical model was constructed based on simple conservation of energy arguments and an instability model. Several simplifying assumptions were made. The analytical model performed relatively well for the closed shaft with reasonable agreement between predicted and experimental values. For the vented channels, although the model produced temperature profiles that were qualitatively similar to the test data, the agreement was not as good. It is evident that the gas withdrawal from opening on the side of the shaft causes the flow no longer to be one-dimensional near the window.

Many types of models exist for the prediction of fire behavior and smoke transport

in a building. The zone model CFAST discussed in chapter 1 is an example. Flow in a vertical shaft with a high aspect ratio cannot be simulated well with the two-layer assumption in most zone type models. The experimental data from this study can aid in the development of these fire modeling codes. Specifically the model developed by Cooper (1994) for high aspect ratio shafts can be expanded to include heat transfer effects and flow through vents.

More computational studies and flow visualization experiments pertaining to smoke movement in vertical shafts are necessary to better understand the behavior of toxic products caused by high-rise building fires.

References

1. Avallone, E.A., and Baumeister, T., editors, 1987, *Marks' Standard Handbook for Mechanical Engineers*, 9th ed., McGraw Hill, New York

2. Brown, C.K., and Gauvin, W.H., 1965, *Combined Free and Forced Convection*, Canadian Journal of Chemical Engineering, v. 43, pp 306-318

3. Bruun, H.H., 1995, *Hot Wire Anemometry: Principles and Signal Analysis*, Oxford University Press

4. Buckley, J.B., 1985, *High-Rise Fire Safety Systems*, ASHRAE Journal, v.27, no. 4, pp 26-29

5. Cooper, L., 1994, *Simulating Smoke Movement Through Long Vertical Shafts in Zone-Type Compartment Fire Models*, NISTIR 5526, Building and Fire Research Laboratory, National Institute of Standards and Technology

6. Cannon, J.B., 1975, *Convective Flows Under Conditions Applicable to Fires in High Rise Buildings*, Ph.D. Thesis, California Institute of Technology, Pasadena, CA

7. Drysdale, D., 1985, *An Introduction to Fire Dynamics*, John Wiley and Son, New York

8. Emmons, H.W., 1983, *The Calculation of a Fire in a Large Building*, Transactions of the ASME: Journal of Heat Transfer, v. 105, pp 151-158

9. Emmons, H.W., 1988, *Why Fire Model: The MGM Fire and Toxicity Testing*, Fire Safety Journal, v. 13, no. 2, pp77-85

10. Fisher, H.B., Imberger, J., List, E.J., Koh, R.C.Y., and Brooks, N.H., 1979, *Mixing in Inland and Coastal Waters*, Academic Press, New York

11. Fox, R.W., and McDonald, A.T., 1985, *Introduction to Fluid Mechanics*, 3rd Ed., Wiley, New York

12. Hall, J.R., 1997, *The Low-Down on High-Rise Fires*, NFPA Journal, v. 91, no. 6, pp 84-90

13. He, Y., Beck, V., 1997, *Smoke Spread Experiment in a Multi-Storey Building and Computer Modeling*, Fire Safety Journal, V. 28, no. 2, pp 139-164

14. Holman, J.P., 1966, *Experimental Methods for Engineers*, 2nd ed., McGraw-Hill, New York

15. Incropera, I.P., and De Witt, D.P., 1990, *Fundamentals of Heat and Mass Transfer*, 3rd ed., Wiley, New York

16. Jones, W.W., and Forney, G.P., 1993, *Improvements in Predicting Smoke Movement in Compartmented Structures*, Fire Safety Journal, v.21, no.4, pp 269-297

17. Karter, M.J., 1997, *1996 U.S. Fire Loss*, NFPA Journal, v.91, no.5, pp 76-83

18. Kim, S.Y., and Jaluria, Y., 1998, *Combined Buoyancy-Induced and Forced Flow in a Vertical Shaft*, Proceedings of the 7th AIAA/ASME Joint Thermophysics and Heat Transfer Conference, v.2, pp 11-21

19. Lemieux, G.P., and Oosthuizen, P.H., 1985, *A Simple Approach to the Compensation of Constant Temperature Hot-Wire Anemometers for Fluid Temperature Fluctuations*, Instrument Society of America, v.25, no.2, pp 69-72

20. Lyons, J.W., 1985, *Fire*, Scientific America Library

21. Marshall, N.R.,1984, *The Behavior of Hot Gases Flowing within a Staircase*, Fire Safety Journal, v.9, pp 245-255

22. Mcguire, J.H., and Tamura, G.T., 1975, *A Simple Analysis of Smoke Flow Problems in High-Rise Buildings*, Fire Technology, v. 11, no. 1, pp 15-22.

23. Mercier, G.P., and Jaluria, Y., 1995, *Fire-Induced Flow of Smoke in Open Vertical Shafts*, Symposium in Thermal Sciences and Engineering in Honor of Chancellor Chang-Lin-Tien, pp 261-268

24. Ostrach, S., 1988, *Natural Convection in Enclosures*, Transactions of the ASME: Journal of Heat Transfer, v. 110, pp 1175-1190

25. Paul, R.V., 1984, *The High Rise: Trends and Development in Smoke Control*, ASHRAE Journal, v. 26, no. 9, pp 28-30

26. Peacock, R.D., Fornery, G.P., Reneke, P.A., Portier, R.W., and Jones, W.W., 1993, *CFAST, The Consolidated Model of Fire Growth and Smoke Transport*, Technical Note 1299, National Institute of Standards and Technology, Gaithersburg, MD

27. Omega Engineering Inc., 1992 *The Omega Temperature Handbook*

28. Shih, A.C.H., 1994 *The Study of Taylor Coutte Flow with Super-Imposed Isothermal and Heated Axial Flows at High Taylor Numbers*, Phd Thesis, California Institute of Technology, Pasadena, CA

29. Tamura, G.T., 1982 *A Smoke Control System for High-Rise Office Buildings*, ASHRAE Journal, v. 24, no. 5, pp 29-32

30. White, F.M.,1994, *Fluid Mechanics*, 3rd Ed., McGraw Hill, New York

31. Yang, K.T, 1987, *Natural Convection in Enclosures*, Handbook of Single-Phase Heat Transfer, editors: Kakac,S., Shah, R.T., Aung, W., Ch. 13, Wiley, New York

32. Zicherman, J., Scawthorn D., and Sfintesco, D., editors, Council on Tall Buildings and Urban Habitat, 1992, *Fire Safety in Tall buildings*, McGraw-Hill, New York

33. Zukoski, E.E., and Kubota, T., 1980, *Two-layer Modeling of Smoke Movement in Building Fires*, Journal of Fire and Material, v. 4, p. 17

34. Zukoski E.E.,1985, *The Fluid Dynamical Aspects of Fires*, Proceedings of the First International Symposium of Fire Safety Science, Berkeley, CA, pp 1-30

35. Zukoski, E.E., 1995, *A Review of Flows Driven by Natural Convection in Adiabatic Shafts*, NIST-GCR-95-679, National Institute of Standards and Technology, Gaithersburg, MD

Appendix A: Matlab Program

```
% Model
zspan = [0.00  0.23   0.42   0.61  0.79  1.00]'
% Define initial conditions
Tprime0 = -0.634;
T0 = [ 0.253  Tprime0]';
% M- File temp3.m defines ode
[z,T] = ode23('temp3', zspan, T0)

% Define initial conditions
Tprime0a = -0.914;
T0 = [ 0.271 Tprime0a]';
% M- File temp4.m defines ode
[z,Ta] = ode23('temp4', zspan,T0);

% Plot Results
plot(z,T, '-', z,Ta,'--'); grid;
axis([0 1 0 0.3]);
set(gca,'fontsize',13)
[a,b] = legend('H/w=10.2  c=4.47','', 'H/w=17  c=8.96')

set(gca, 'fontsize', 16)
xlabel('Normalized Height, \zeta = z/H')
ylabel('Normalized Temperature, \tau = T/T_i - 1')
%bx=mean(get(b(1,1),'XData'));
%by=mean(get(b(1,1),'YData'));
%set(b(1,1),'XData',bx,'YData',by);
```

```
for i=2;
  bx=mean(get(b(i,1),'XData'));
  by=mean(get(b(i,1),'YData'));
  set(b(i,1),'XData',bx,'YData',by);
end
```

Appendix B: Flow Visualization

A simple smoke wire flow visualization study was performed for the closed channel. The experimental setup is shown in fig. B.1.

One of the aluminum side panels of the channel is replaced with one made of plexiglass. Three 30 gage copper wires were placed horizontally in the channel and were coated with paraffin oil. When an electric current was passed through the wires the smoke evaporated and formed streamlines which characterize the local flow patterns. The back wall of the channel was covered with black paper and a 25 W halogen lamp was used to illuminate the flow. The smoke patterns were recorded by a video camera.

Although the smoke wire produced vertical streamlines in a quiescent flow, when the hot reservoir gas and the cold ambient air were mixing the streamlines dissipated within a few centimeters above the heated smoke wire. This indicated that the flow was very turbulent. Also in some instances the streamlines would be initially directed downward implying that cold gases were moving down in some parts of the duct.

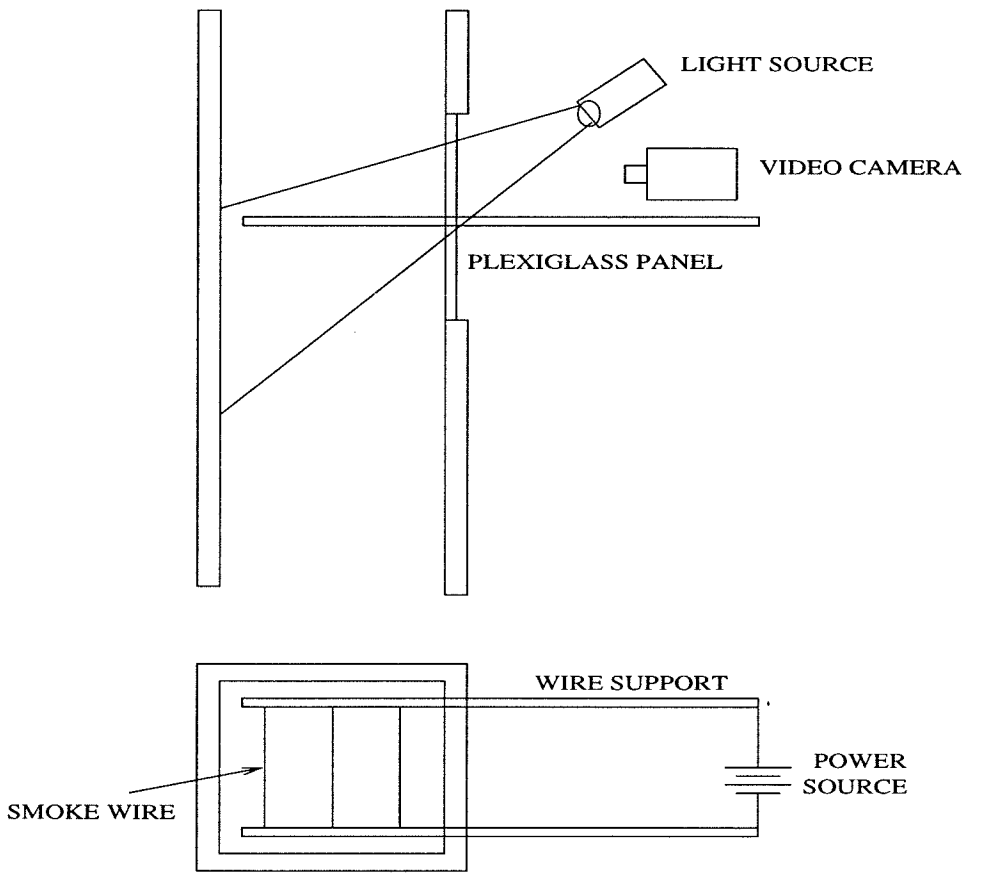

FIG. B.1: Smoke Wire Flow Visualization System

Appendix C: Sample Calculations

Considering the vented channel experiment for $w = 15.24$ cm, $Re_{w,avg} = 3937$ at $z/w = 7.2$.

Experimental Results:

$$T = 71.1^oC;\ T_w = 29.8^oC;\ q_w = 335W/m^2;\ \dot{m} = 0.011kg/s$$

Therefore, the film temperature $T_f = (T + T_w)/2 = 54.5^o$C. The fluid properties evaluated at T_f from Incropera and DeWitt (1990) are

$$\rho = 1.077kg/m^3;\ \nu = 1.72x10^{-5}m^2/s;\ k = 0.0283W/m/K;\ Pr = 0.7$$

The cross-sectional area of the channel is w^2. Hence the local mean velocity is given by,

$$\overline{u} = \frac{\dot{m}}{\rho w^2} = 0.44m/s$$

and the local Reynolds number $Re = \overline{u}w/\nu = 3896$.

Since the wall heat transfer $q_w = 335\ W/m^2$, the heat transfer coefficient, $h = q_w/(T - T_w) = 6.85\ W/m^2/K$. Thus

$$Nu = \frac{hw}{k} = 36.9$$

Now,

$$Gr = \frac{g\beta(T - T_w)w^3}{\nu^2}$$

where,

$$\beta = \frac{1}{\rho}\frac{\partial\rho}{\partial T} = \frac{1}{T_f}$$

for an ideal gas. Hence $Gr = 1.76\text{x}10^7$ and from the experimental correlation (4.2)

$$Nu_w = 0.18(Gr_wPr)^{1/3} = 41.6$$